

MODIFICATION OF METAL PHOSPHONATE MONOLAYERS AND THE EFFECT ON  
INTERFACIAL ORGANIZATION AND TRANSLATIONAL DYNAMICS

By

Corbin Livingston

A DISSERTATION

Submitted to  
Michigan State University  
in partial fulfillment of the requirements  
for the degree of

Chemistry – Doctor of Philosophy

2021

## ABSTRACT

### MODIFICATION OF METAL PHOSPHONATE MONOLAYERS AND THE EFFECT ON INTERFACIAL ORGANIZATION AND TRANSLATIONAL DYNAMICS

By

Corbin Livingston

Self-assembled monolayers (SAMs) are used widely for surface modification due to the range of chemical structures available and the comparative ease of synthesis. In particular, metal-phosphonate and metal bisphosphonate (MP) films have received attention for several decades. MP films were first described using zirconium but have since been expanded to include other metals including many group II metals, first and second row transition metals, and many lanthanides, with a variety of oxidation states represented. While the structural properties of MP films have been characterized thoroughly and reported, the dynamics within MP film have not received much attention. The focus of this dissertation is on determining the surface organization and translational dynamics of MP monolayers.

Due to the large variability in MP films, modifications of traditional ZP monolayers and the effects of constituent dynamics are reported here. The effect of metal ion charge and identity on the metal ion complexation equilibria and exchange kinetics, and surface organization were investigated. Many reported MP monolayers are formed using an  $\alpha,\omega$ -alkanebisphosphonate, however this constituent can be easily substituted or modified for a variety of applications. Reported here is the effect of constituent modification on the constituent exchange dynamics and consequent translational mobility within MP monolayers.

## ACKNOWLEDGEMENTS

There are so many people that have been incredibly influential throughout the course of my time at Michigan State that I will inevitably leave someone out, but that's all to say that I did not do this alone, and am grateful for all of those who have helped me along the way. Most notably, my advisor Dr. Gary Blanchard has served as a diligent, generous, and unwavering support through my graduate career and thank him immensely for his role. I would like to express my gratitude to my committee; Dr. James McCusker, Dr. Tom Hamann, and Dr. Greg Swain. Thank you all for your guidance and support.

I would also like to thank my fellowship advisor Dr. Rachel Barnard for serving as an incredible mentor, introducing me to chemistry education research, and always being available for career advice. I have been fortunate to have many great lab mates and colleagues along the way that have been influential in and out of lab. Specifically, Briana Capistran, Dr. Dhvani Kansal, Dr. Kelly Aldrich, and all of the past members of the Blanchard group.

My family and friends have been immensely supportive and gracious throughout this entire process and I could not be more thankful, so thank you all, but special thanks to my parents and Erik.

## TABLE OF CONTENTS

LIST OF TABLES.....	v
LIST OF FIGURES .....	vi
Chapter One: Introduction .....	1
REFERENCES .....	6
Chapter Two: Metal Ion Dependent Interfacial Organization and Dynamics of Metal- Phosphonate Monolayers .....	9
2.1 Abstract.....	10
2.2 Introduction.....	10
2.3 Experimental.....	12
2.4 Results and Discussion .....	15
2.5 Conclusions.....	27
APPENDIX.....	29
REFERENCES .....	32
Chapter Three: Translational Diffusion Dynamics in Divalent Metal Phosphonate Monolayers .....	37
3.1 Abstract.....	38
3.2 Introduction.....	38
3.3 Experimental.....	40
3.4 Results and Discussion .....	43
3.5 Conclusions.....	56
REFERENCES .....	58
Chapter Four: Effect of Monolayer Constituent Structural Modification on the Constituent Diffusional Properties of Metal Phosphonate Monolayers .....	62
4.1 Abstract.....	63
4.2 Introduction.....	63
4.3 Experimental.....	66
4.4 Results and Discussion .....	67
4.5 Conclusions.....	76
REFERENCES .....	77
Chapter Five: Conclusions and Future Work.....	81
REFERENCES .....	87

## LIST OF TABLES

Table 2-1. Translational diffusion constant ( $D_T$ ) for metal-bisphosphonate monolayers with an untethered chromophore (perylene). Viscosity values are determined using Eq. 4. ....	23
Table 2-2. Translational diffusion constants ( $D_T$ ) for metal-bisphosphonate monolayers with a tethered chromophore, BPDI. ....	27
Table 3-1. Thickness measurements from ellipsometric measurements. ....	45
Table 3-2. Average $D_T$ values and calculated viscosities for MP monolayers with an untethered chromophore. ....	50
Table 3-3. $D_T$ values for M(II)P monolayers with a tethered chromophore at varying bleach radii ( $w$ ) showing no dependence. ....	53
Table 3-4. $D_T$ and $k_{on}^*$ and $k_{off}$ values for MP monolayers with a tethered chromophore. ....	55
Table 4-1. $D_T$ values for MP monolayers with a tethered chromophore. ....	68
Table 4-2. Average $D_T$ values and calculated viscosities for MP monolayers with an untethered chromophore. ....	69
Table 4-4. Average $D_T$ values and calculated viscosities for MP monolayers with the terminal phosphonate removed with an untethered chromophore. For purposes of comparison, the viscosity of glycerol is <i>ca.</i> 1410 cP at room temperature. ....	74
Table 4-5. Average $D_T$ values and calculated viscosities for MP monolayers with a 12 carbon aliphatic chain with an untethered chromophore. For purposes of comparison, the viscosity of glycerol is <i>ca.</i> 1410 cP at room temperature. ....	76
Table 5-1. $D_T$ values for MP monolayers with a tethered chromophore. ....	82
Table 5-2. Average $D_T$ values for MP monolayers with an untethered chromophore. ....	83

## LIST OF FIGURES

Figure 2-1. Schematic of metal-phosphonate monolayer synthesis.....	13
Figure 2-2. Synthesis of N,N'-bis(4-phosphonobutyl)-3,4,9,10-perylenediimide (BPDI). The reaction was performed in imidazole, with no solvent added.....	14
Figure 2-3. Diagram for Fluorescence Recovery After Photobleaching (FRAP) instrument.....	15
Figure 2-4. (a) Metal-bisphosphonate monolayers on silicon used to determine film thickness. (b) Idealized representation of Zr-bisphosphonate sheets with estimated layer length.....	17
Figure 2-5. Model of a metal-bisphosphonate monolayer with perylene on a glass substrate. ....	20
Figure 2-6. Plot of time (s) vs. relative intensity. These data was obtained from a single FRAP experiment with perylene. Recovery curves do not show 100% recovery due to the photodegradation of the chromophore overtime. Grey squares represent residuals for each recovery curve.....	21
Figure 2-7. Model of metal-bisphosphonate with BPDI on a glass substrate.....	24
Figure 2-8. Plot of time (s) vs. relative intensity. This data was obtained from a single FRAP experiment with BPDI. Grey squares represent residuals for each recovery curve.....	25
Figure A2-1. Structure of tethered chromophore BDPI.....	30
Figure A2-2. Absorption spectrum of BDPI. $\lambda_{\max}$ :484nm.....	30
Figure A2-3. Emission spectrum of BDPI. $\lambda_{\max}$ : 668nm.....	31
Figure 3-1. Schematic of MP monolayer synthesis. ....	41
Figure 3-2. Schematic of phosphonate monolayer synthesis.....	42
Figure 3-3. Perylene incorporated in a MP monolayer. The protonation of the oxygens involved in metal binding depends on charge balance and for the sake of clarity are shown unprotonated here.....	46
Figure 3-4. Plot of time (s) vs. relative intensity. These data was obtained from a single FRAP experiment with perylene in an MP monolayer. Grey squares represent residuals for each recovery curve.....	48
Figure 3-5. BDPI incorporated in a MP monolayer. The protonation of the oxygens involved in metal binding depends on charge balance and for the sake of clarity are shown unprotonated here.....	52

Figure 3-6. Plot of time (s) vs. relative intensity. These data was obtained from a single FRAP experiment with BDPI in an MP monolayer. Grey squares represent residuals for each recovery curve.....54

Figure. 4-1. Schematic of metal-phosphonate monolayer. The protonation of the oxygens involved in metal binding depends on charge balance and for the sake of clarity are shown unprotonated here.....64

Figure 4-2. Scheme of ZP films with oligothiophene chromophores.....65

Figure 4-3. BDPI incorporated in a MP monolayer. The protonation of the oxygens involved in metal binding depends on charge balance and for the sake of clarity are shown unprotonated here.....67

Figure 4-4. Perylene incorporated in a MP monolayer. The protonation of the oxygens involved in metal binding depends on charge balance and for the sake of clarity are shown unprotonated here.....69

Figure 4-5. Tail-end modification of MP monolayers including extending the aliphatic chain length, metal capping, and removing the terminal phosphonate. ....70

Figure 4-6. Plot of time (s) vs. relative intensity of metal capped MP monolayers. These data were obtained from a FRAP measurement using perylene as the untethered chromophore. ....73

Figure 4-7. Plot of time (s) vs. relative intensity of MP monolayers with the terminal phosphate removed. These data was obtained from a single FRAP experiment with perylene. ....75

Figure 5-1. Structure of LB film incorporating a metal, phospholipid (1,2-dimyristoyl-sn-glycero-3-phosphcholine), and a tethered chromophore. ....84

Figure 5-2. Scheme of mixed metal MP multilayer.....85

## **Chapter One: Introduction**

Self-assembled monolayers are a surface modification that is attractive for many applications due to the ease of synthesis and versatility of constituents. Langmuir-Blodgett (LB) films were developed prior to the development of SAMs. While LB films are still used today and have many benefits, LB films require the use of advanced instrumentation and there are solvent and solubility limitations. SAMs offer an analogous surface modification, but without the use of advanced instrumentation, and fewer solubility constraints. In addition, SAMs can be bound to the support surface by any of several chemical means, all of which are characterized by a greater binding energy than is achievable with LB films. SAMs are made by the sequential addition of monolayer constituents, allowing versatility. Self-assembled monolayers were largely developed in the 1980s and 1990s, with many groups modifying the synthesis and structure to fit their needs. This made for a robust body work featuring many SAMs that are fully characterized and easily synthesized.

The work that follows is focused on self-assembled metal-phosphonate and metal-bisphosphonate monolayers. Initially, MP monolayers were made with Zr(IV). These Zr-bisphosphonate (ZP) layers are initiated from a phosphate- or phosphonate-terminated surface, that a metal is then complexed to, followed by exposure to a phosphonate. The use of  $\alpha,\omega$ -bisphosphonates as layer constituents allows for the formation of multilayer structures in a stepwise process. Multilayers into the hundreds have been reported, where the metal and then bisphosphonate steps are repeated until the desired length is reached. Though multilayers are stable and robust, the focus of this work is on monolayers. The Mallouk and Thompson groups pioneered much of the early ZP work. ZP layers have been optimized for use broadly as surface modification agents for specific applications, including small molecule sensing, molecular recognition applications, polymer coatings, and oligonucleotide microarrays.<sup>1-3</sup> Thorough

structural characterization of ZP films has been reported. Ellipsometric measurements were consistent with the growth of macroscopically uniform layers where the alkyl chains of the bisphosphonates are all-*trans*. Variable take-off angle XPS<sup>4</sup> has shown that the films exist as compact layers. X-ray powder diffraction shows a “well-ordered” film with few defects.<sup>5</sup> AFM shows the deposition of a uniform film with roughness of the bisphosphonate monolayer commensurate with that of the zirconated surface.<sup>6</sup> Previous members of the Blanchard group explored the motional dynamics of ZP thiophene oligomer monolayers using time-resolved spectroscopy. It was found that the bisphosphonate exhibits a  $\sim 35^\circ$  tilt angle and rotational motion is apparent in ZP monolayers.<sup>7</sup> The Blanchard group has also further examined the excitation transfer dynamics within those ZP films and found that the ZP complex acted as an effective dielectric barrier to inter-layer excitation transport.<sup>8, 9</sup>

While the initial focus of metal-bisphosphonate films was Zr(IV), many other MP films have since been described. Other tetravalent, trivalent, and divalent metal bisphosphonate layers have been reported in the literature. The ratio of metal: bisphosphonate is 2:1 regardless of the formal charge on the metal ion.<sup>10, 11</sup> When the charge on the metal is less than four, the charge is balanced by protonation of the phosphonate moieties or the addition of counterions.<sup>11</sup> It has been shown that the coordination geometries of monolayers mimic those of the analogous bulk metal bisphosphonate compound.<sup>12</sup> While the structure of MP films incorporating various metals has been thoroughly investigated, there is little in the literature that addresses the translational diffusion dynamics that are characteristic of MP films and, specifically, how these dynamics depend on the metal ion used in monolayer formation.

SAMs are typically compared to Langmuir-Blodgett (LB) films. LB monolayers are formed on a liquid subphase and subsequently deposited onto a solid support where

physisorption is the extent of monolayer-surface interaction.<sup>13</sup> This means monolayer formation requires the use of a LB trough to form the monolayer and then deposit it onto a surface. SAMs do not require the use of such dedicated instrumentation for assembly. While LB films rely on relatively weak interactions between the surface and monolayer, SAMs are chemically bonded to the surface, either through covalent bonding or metal ion complexation. This structural distinction influences the properties of each type of film. Here, the focus will be on the fluid properties of thin films, which will be described using the translational dynamics of the monolayer constituents.

The diffusion of monolayer constituents within LB films has been previously described by the Blanchard group.<sup>14-16</sup> In that work, phospholipid monolayers were created using the LB technique and were supported on a phosphorylated glass surface. The translational diffusion dynamics of LB film constituents was probed using fluorescence recovery after photobleaching (FRAP) measurements.<sup>14</sup> While LB monolayers are physisorbed to the surface, allowing translational diffusion and covalently bound surface modifications do not allow translational movement, the metal complexation in MP films offers an alternative to LB films as a medium exhibiting some translational freedom because the metal ion complexation is an equilibrium process, where both association and dissociation operate.

Controlling the fluid properties of the MP interface would afford a synthetically simple surface modification with broad applications from in tribology to chemical sensing. One notable example is within tribology which is the modification of frictional properties. One common method for reducing the friction between two solid surfaces is to insert a liquid at the interface. This is the basic principle for lubrication. However, this is not a suitable solution for many

systems that are friction limited. Employing a surface modification that would act as a liquid at the interface could be used more broadly and particularly within high precision applications.

MP monolayers offer as surface modification that is easily formed on the benchtop, highly tunable, and requires limited instrumentation. The overall goal is to determine if MP films exhibit surface fluidity and if modifications to the monolayers result in increased fluidity. The research questions for this project are three-fold.

1. Do ZP films exhibit surface fluidity?

How does metal ion charge and identity effect the surface fluidity of MP films?

2. How does end group identity effect the surface fluidity of MP films?

In Chapter 2, the molecular dynamics and organization of traditional ZP films is reported. An analogous In(III)-bisphosphonate monolayers was assembled, characterized, and analyzed in order to determine how changing the metal ion charge from  $4^+$  to  $3^+$  affects the translational diffusion of the monolayer. Chapter 3 focuses on reducing the metal ion charge in MP films to  $2^+$ , and also on metal ion identity and how these changes affect the molecular dynamics of the films. In Chapter 4, modifications of the end group constituent are explored and the effect on monolayer diffusion.

## **REFERENCES**

## REFERENCES

1. Mallouk, T. E.; Gavin, J. A., Molecular recognition in lamellar solids and thin films. *Accounts of Chemical Research* **1998**, *31* (5), 209-217.
2. Kohli, P.; Blanchard, G. J., Design and growth of robust layered polymer assemblies with molecular thickness control. *Langmuir* **1999**, *15* (4), 1418-1422.
3. Lane, S. M.; Monot, J.; Petit, M.; Bujoli, B.; Talham, D. R., XPS investigation of DNA binding to zirconium-phosphonate surfaces. *Colloid Surface B* **2007**, *58* (1), 34-38.
4. Akhter, S.; Lee, H.; Hong, H. G.; Mallouk, T. E.; White, J. M., Structural characterization of multilayer metal phosphonate film on silicon using angular-dependent x-ray photoelectron spectroscopy. *Journal of Vacuum Science & Technology A* **1989**, *7* (3), 1608-1613.
5. Hong, H. G.; Sackett, D. D.; Mallouk, T. E., Adsorption of well-ordered zirconium phosphonate multilayer films on high surface area silica. *Chemistry of Materials* **1991**, *3* (3), 521-527.
6. Byrd, H.; Snover, J. L.; Thompson, M. E., Mechanistic Studies of Film Growth of Zirconium Bis(Phosphonate) Monolayer and Multilayer Thin-Films - These Things Grow Darned Flat. *Langmuir* **1995**, *11* (11), 4449-4453.
7. Horne, J. C.; Blanchard, G. J., Dynamics within a single molecular layer. Aggregation, relaxation, and the absence of motion. *J Am Chem Soc* **1996**, *118* (50), 12788-12795.
8. Horne, J. C.; Blanchard, G. J., The role of substrate identity in determining monolayer motional relaxation dynamics. *J Am Chem Soc* **1998**, *120* (25), 6336-6344.
9. Horne, J. C.; Huang, Y.; Liu, G. Y.; Blanchard, G. J., Correspondence between layer morphology and intralayer excitation transport dynamics in zirconium-phosphonate monolayers. *J Am Chem Soc* **1999**, *121* (18), 4419-4426.
10. Cao, G.; Lee, H.; Lynch, V. M.; Mallouk, T. E., Synthesis and structural characterization of a homologous series of divalent-metal phosphonates,  $MII(O_3PR)_2 \cdot nH_2O$  and  $MII(HO_3PR)_2$ . *Inorg Chem* **1988**, *27* (16), 2781-2785.
11. Cao, G.; Lynch, V. M.; Swinnea, J. S.; Mallouk, T. E., Synthesis and Structural Characterization of Layered Calcium and Lanthanide Phosphonate Salts. *Inorg Chem* **1990**, *29* (11), 2112-2117.
12. Sagiv, J., Organized monolayers by adsorption. II. Molecular orientation in mixed dye monolayers built on anisotropic polymeric surfaces. *Israel Journal of Chemistry* **1980**, *18* (3-4), 339-45.

13. Blodgett, K. B., Films Built by Depositing Successive Monomolecular Layers on a Solid Surface. *J Am Chem Soc* **1935**, 57 (6), 1007-1022.
14. Baumler, S. M.; Blancharde, G. J., The Influence of Metal Ions on the Dynamics of Supported Phospholipid Langmuir Films. *Langmuir* **2017**, 33 (12), 2986-2992.
15. Baumler, S. M.; McHale, A. M.; Blanchard, G. J., Surface charge and overlayer pH influence the dynamics of supported phospholipid films. *J Electroanal Chem* **2018**, 812, 159-165
16. Baumler, S. M.; Reidy, T. M.; Blanchard, G. J., Diffusional motion as a gauge of fluidity and interfacial adhesion. Supported alkylphosphonate monolayers. *J Colloid Interf Sci* **2016**, 468, 145-155.

## **Chapter Two: Metal Ion Dependent Interfacial Organization and Dynamics of Metal-Phosphonate Monolayers**

## 2.1 Abstract

Self-assembled monolayers have been studied extensively due to their relative ease of synthesis and the broad range of applications for this class of materials. Monolayer-support interactions can range in strength from physisorption through covalent bond formation, with consequent variability in the robustness and fluidity of the monolayer. Monolayer-support bonding by metal ion complexation is especially attractive because of the ability to adjust the strength of interaction through metal ion identity. For such systems, both the exchange kinetics and thermodynamics of metal ion-complex formation contribute to the observed properties of the monolayer. We have synthesized metal phosphate/phosphonate monolayers using  $Zr^{4+}$  and  $In^{3+}$  and have evaluated the metal ion dependence of monolayer dynamics for free and bound chromophores. Our findings reveal significant metal ion-dependent variations in monolayer dynamics and organization.

## 2.2 Introduction

Self-assembled monolayers (SAMs) have attracted wide attention because of their ability to modify the properties of interfaces.<sup>17-20</sup> SAMs are characteristically formed using amphiphilic molecular species and the means of growth and bonding to the surface of the support play deterministic roles in the properties of the resulting monolayer.<sup>17-19, 21, 22</sup> We are interested in the permeability and fluidity of monolayers because of their importance in chemical sensing and separations applications, and for their potential utility in modifying the frictional properties of interfaces. For our intended purposes, the monolayer structures of interest must be relatively robust. While the formation and deposition of monolayers using Langmuir-Blodgett technology is well developed and is known to produce highly ordered monolayers, the chemical interactions

between the support surface and the amphiphile monolayer are not sufficiently robust for many applications.<sup>13</sup> Conversely, covalent bonding of monolayers onto support surfaces renders the monolayer constituents immobile and therefore of limited utility for our intended purposes. The formation of monolayers using metal ion complexation to bind the monolayer to the support surface is somewhat more complex structurally than either physisorbed or covalent monolayers.<sup>7, 11, 23-28</sup> However, this structural motif has the advantage of being an equilibrium (i.e. dynamic) system with respect to interactions between the monolayer and the support. In addition, through sufficiently high thermodynamic driving force, these SAMs can also be robust. Another useful property of monolayers formed by complexation is that the monolayer itself is fluid, rather than solid, resulting in structures that may be characterized by low defect densities.<sup>16</sup>

As noted above, the properties of primary interest for our intended applications are the fluidity and permeability of the monolayer. Monolayers formed using metal ion complexation chemistry exhibit structures and strength of bonding that depend on the metal ion and complexing agent(s) used. In this work, we use phosphate-terminated support surfaces and monolayer constituents containing terminal phosphonate functionalities. The complex of interest is the phosphate-metal-phosphonate moiety. The equilibrium constants for these complexes are, in general, not known but are expected to correlate with those of the corresponding metal bisphosphate structures. What is not generally known for these systems is how the metal ion coordination with surface phosphate functionalities is affected by the enforced geometric constraints of the nominally planar support, and association and dissociation kinetics for the complex.

Metal bisphosphonate SAMs, particularly those using  $Zr^{4+}$  and  $Hf^{4+}$ , are well known and have been characterized extensively.<sup>23-26, 29-31</sup> The synthesis of these monolayers is

straightforward and they form relatively stable interfacial assemblies.<sup>23</sup> Despite the extensive literature on the characterization of the structural properties of these films, including FTIR, XPS, NMR, AFM, ellipsometry, and crystallographic data on analogous systems and analogous solid state bulk materials,<sup>23, 26, 31-33</sup> there is limited information available on the dynamic properties of these materials. We have investigated molecular mobility within the aliphatic chain region of these monolayer structures as a function of the identity of the metal ion used in their formation. We probe the disorder intrinsic to these monolayer structures resulting from the enforced spacing between the monolayer constituents. This enforced spacing influences the ability of these monolayers to function in applications ranging from chemical sensing and separations to surface lubrication. We use fluorescent probe molecules to investigate the nature of the organic gallery region of the monolayers and the mobility of the monolayer constituents. The issues of free constituent mobility and equilibrium association and dissociation dynamics of the monolayer constituents both play a role in determining monolayer properties. Our data demonstrate that the monolayer film organization and monolayer constituent dynamics both depend on metal ion identity. We use fluorescence recovery after photobleaching (FRAP) measurements to quantitate chromophore diffusional behavior. These data have important implications on the utility of these materials for chemical sensing and tribological applications.

### **2.3 Experimental**

*Chemicals used:* All water was purified using a Milli-Q purification system. Concentrated sulfuric acid, 2,4,6-collidine,  $\text{In}(\text{NO}_3)_3 \cdot x\text{H}_2\text{O}$ , and 1,8-octanediphosphonic acid were obtained from Sigma-Aldrich and used without further purification. Aminiobutylphosphonic acid was obtained from ChemScene and used without further

purification. 3,4,9,10-Perylenetetracarboxylic dianhydride was obtained from TCI and used without further purification.

*Metal bisphosphonate monolayer synthesis.* Glass or oxidized silicon plates (1cm x 1cm), used as monolayer supports, were cleaned by immersion in piranha solution (*Caution! Strong oxidizer!*) for 15 minutes.<sup>7</sup> The plates were then rinsed with 18 MΩ water and immersed in a 2M HCl solution. The plates were rinsed with 18 MΩ water and then with anhydrous acetonitrile. The surface was phosphorylated by immersion in 100 mM POCl<sub>3</sub> (*Caution! Evolves HCl when exposed to air, use in a fume hood*) and 100 mM 2,4,6-collidine, a Lewis base, in dry acetonitrile for one hour, then rinsed with anhydrous acetonitrile. The plates were then treated overnight with 5 mM metal ion solution, ZrOCl<sub>2</sub> or In(NO<sub>3</sub>)<sub>3</sub> x H<sub>2</sub>O in 60% EtOH/ 40% H<sub>2</sub>O. The pH was maintained between 2 and 4 using dilute HCl to minimize the formation of metal hydroxides. After washing with Milli-Q water, the plates were treated with 1.25 mM 1,8-octanediphosphonic acid in 95% EtOH for one hour. For substrates used to perform FRAP measurements, the phosphonate solution contained 1 mol% of the chromophore and was added dropwise to the glass slide until it was covered and allowed to sit open to air for 15-20 minutes (*vide infra*, Figure 2-1).

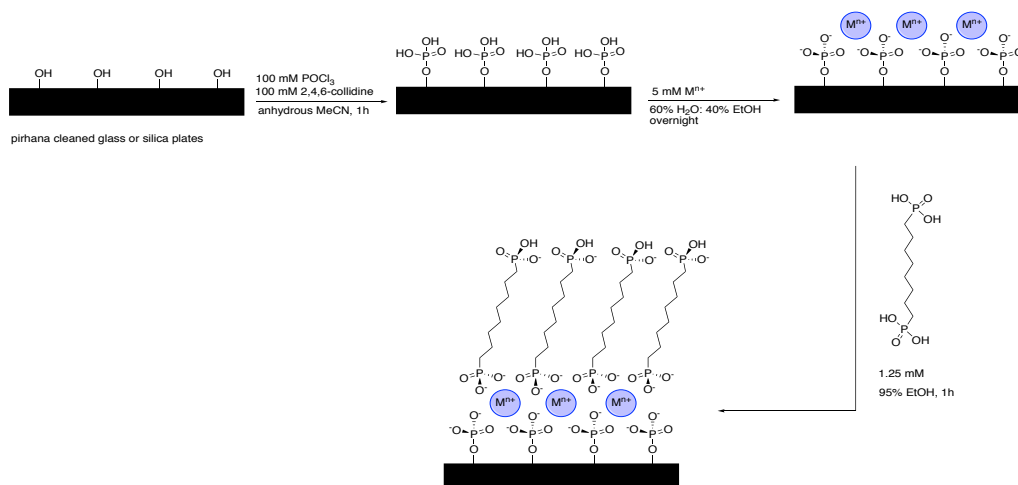


**Figure 2-1. Schematic of metal-phosphonate monolayer synthesis.**

*Tethered chromophore synthesis.* N,N'-bis(4-phosphonobutyl)-3,4,9,10-perylenediimide (BPDI) was synthesized according to the following procedure. 3,4,9,10-Perylenetetracarboxylic dianhydride (0.157 g, 0.4 mmol) was mixed with 2 equivalents of 4-aminobutylphosphonic acid (0.1225g, 0.8 mmol), and excess (0.5 g, 7.3 mmol) imidazole was added to a scintillation vial. The solution was heated to 130°C for 30 minutes, then cooled to room temperature and 10 mL of equal parts EtOH and 2M HCl was added while stirring. Two equivalents of NaOH solution were added and allowed to stir overnight. Excess imidazole was extracted with dichloromethane and water was removed under vacuum prior to lyophilization with toluene.<sup>34</sup> A schematic of the reaction is shown in Figure 2-2. Isolated yield: 34%

<sup>1</sup>H NMR (500 MHz, D<sub>2</sub>O): δ 7.86 (m, 4H), 7.11 (m, 4H), 3.98 (t, 4H), 2.02-1.28 (m, 12H) <sup>31</sup>P

NMR (202 MHz D<sub>2</sub>O): δ 25.37

Absorption  $\lambda_{\max}$ :484nm Emission  $\lambda_{\max}$ : 668nm

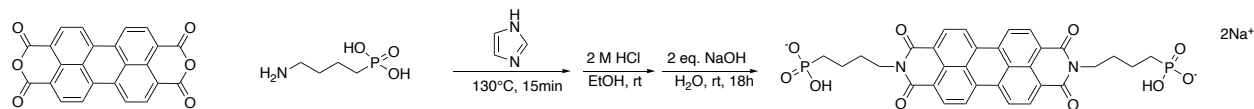


**Figure 2-2. Synthesis of N,N'-bis(4-phosphonobutyl)-3,4,9,10-perylenediimide (BPDI).**

**The reaction was performed in imidazole, with no solvent added.**

*Optical ellipsometry.* A spectroscopic ellipsometer (Gaertner) equipped with a 75 W xenon lamp source and an M-44 detector with an EC110 multiwavelength control module was used to determine film thickness. All thickness measurements were performed on silicon plates cleaned with piranha solution (1H<sub>2</sub>O<sub>2</sub>:3HNO<sub>3</sub>). This preparation method produces ca. 15 Å oxide film which can be phosphorylated and reacted to produce a monolayer as described above. A minimum of ten spots across each substrate were measured, the reported values are the averages of these measurements.

*Fluorescence Recovery After Photobleaching (FRAP).* A Nikon C2+ confocal laser scanning microscopy system with a Nikon Eclipse Ti-E inverted microscope with a confocal scanning system (Nikon Ti-S-CON) was utilized for acquiring FRAP data. A 20× objective lens was used for all experiments. The chromophores were excited at 405 nm or 488 nm with a diode laser (Nikon Lu-N4) and detected using a PMT detector system (Nikon C2-DU3, 400nm-700nm) (Figure 2-3). For perylene the 405 nm diode laser was used for excitation and for BPDI, the 488 nm diode laser was used. For both the tethered and untethered systems, initial intensity was measured for 30 sec, bleached for 5 sec, and recovery was monitored for a minimum of 12 minutes. A minimum of ten spots across each plate were measured in this manner.

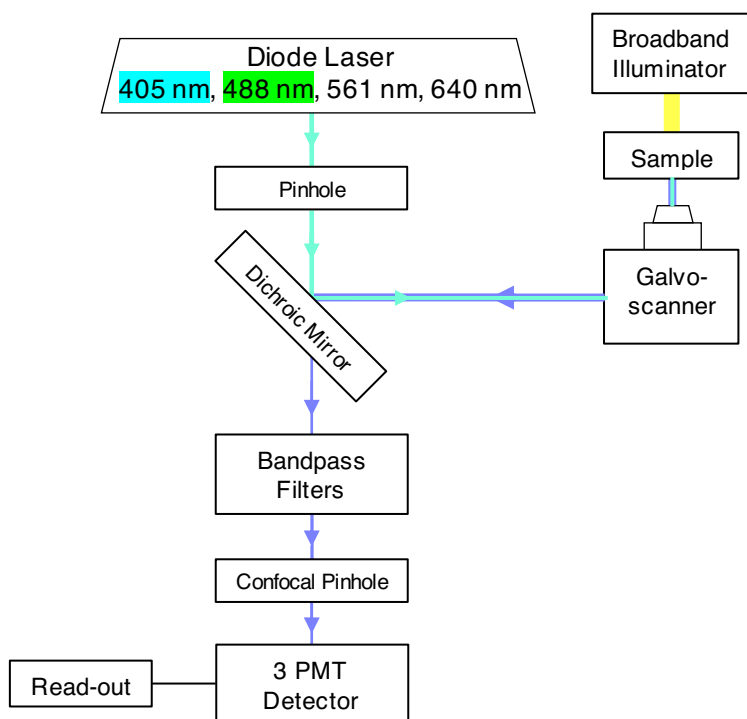


**Figure 2-3. Diagram for Fluorescence Recovery After Photobleaching (FRAP) instrument.**

## 2.4 Results and Discussion

One goal of this work is to determine how the use of two different metal ions ( $Zr^{4+}$  and  $In^{3+}$ ) affects the organization and translational dynamics of metal phosphate/phosphonate

monolayers. We evaluate changes in monolayer packing and organization through optical ellipsometry and translational diffusion measurements of a free chromophore, perylene, within the monolayer. To evaluate the dynamics of the monolayer constituents, we measure the translational diffusion behavior of a tethered chromophore, BPDI. We evaluate the information content of these measurements prior to considering how that information collectively informs our understanding of these monolayers. We selected the two metal ions  $Zr^{4+}$  and  $In^{3+}$  because of the requisite differences in their bonding to the phosphate or phosphonate functionalities both on the support and from the monolayer constituents. Zirconium-bisphosphonate (ZP) monolayers have been studied extensively but a clear understanding of the dynamics that characterize these films remains to be established. Indium bisphosphonate monolayers, in contrast, have received comparatively little attention but provide a comparison to the ZP monolayers using a trivalent metal ion.

*Optical Ellipsometry.* For any MP film, monolayer coverage, uniformity, and order can be challenging to evaluate, especially for monolayers grown on insulating supports such as silica. Ellipsometric measurement of film thickness can at least provide some of the information. For structures that terminate growth at one monolayer, such as those reported in this work, comparison of the measured film thickness to monolayer constituent dimensions can provide an estimate of monolayer coverage (Figure 2-4a). For a  $C_8$  bisphosphonate monolayer bound to the phosphate-modified support through  $Zr^{4+}$  coordination, we estimate the layer thickness to be ca. 23 Å based on molecular mechanics calculations. Experimentally, the ZP monolayer is found to be  $20 \pm 1$  Å and for the InP monolayer  $19 \pm 1$  Å. Due to the similar ionic radii of  $Zr^{4+}$  and  $In^{3+}$ , 0.72 Å and 0.80 Å respectively, the assumption can be made that the films should have the same thickness.<sup>35</sup> The thicknesses obtained experimentally for both films are consistent with

monolayer coverage. Samples of the films were left in water for four days in order to determine the long-term stability. Ellipsometric measurements were taken after the films were left in water for four days with the ZP monolayer being  $20 \pm 1 \text{ \AA}$  and the InP monolayer  $20 \pm 1 \text{ \AA}$  thick.

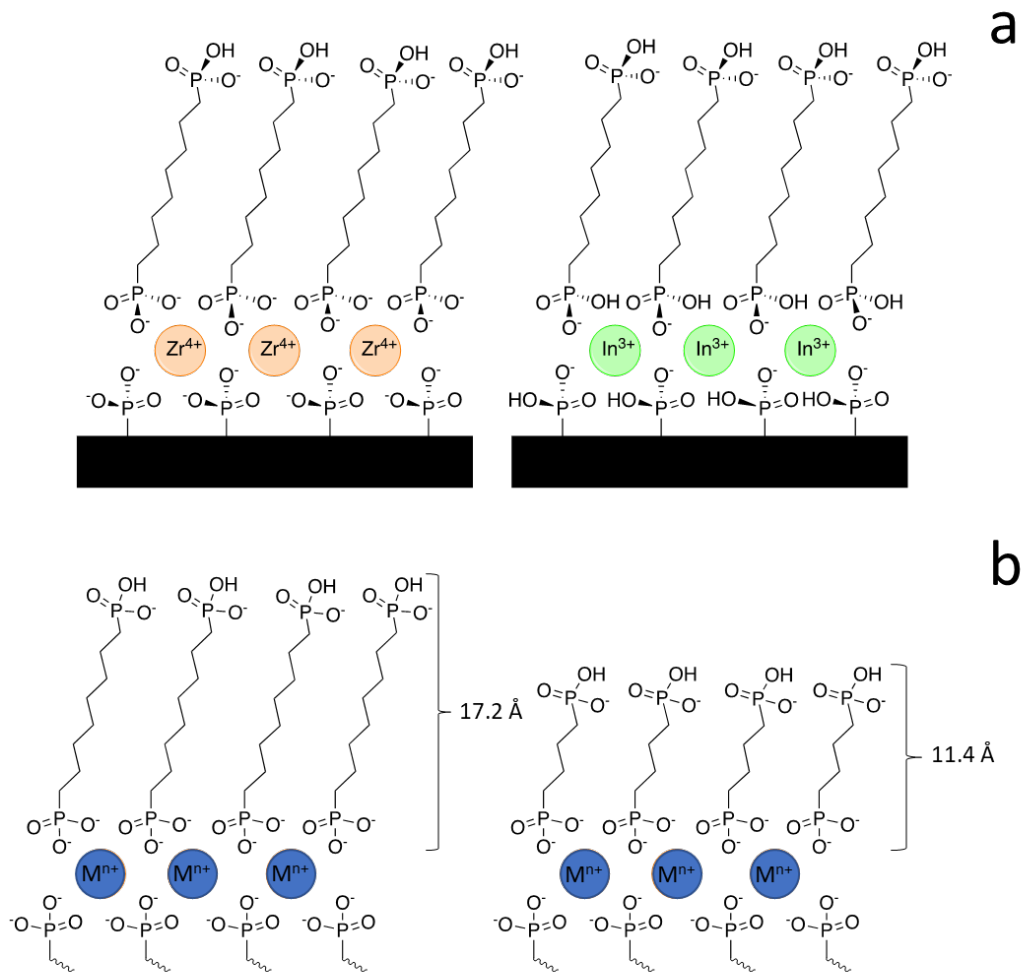


**Figure 2-4. (a) Metal-bisphosphonate monolayers on silicon used to determine film thickness. (b) Idealized representation of Zr-bisphosphonate sheets with estimated layer length.<sup>3</sup>**

Metal-phosphonate 2-D adlayers have been found to exhibit coordination geometries that correspond to analogous 3-D bulk inorganic species.<sup>23</sup> This has been shown to be true with various metal ions across different charge states, including di, tri, and tetravalent metal-

phosphonates. Previous crystallographic studies have shown that divalent, trivalent, and tetravalent metal phosphonates exhibit similar solid-state geometries and are composed of a 1:2 metal to phosphonate ratio,<sup>11, 36</sup> where either the details of the coordination or the presence of counterions will vary with metal ion oxidation state. Zirconium phosphates/phosphonates are characterized by Zr atoms in a plane with phosphate/phosphonate functionalities above and below the metal ion plane, and the phosphate/phosphonate R group nominally perpendicular to the metal ion plane. In multilayer structures, the distance between the Zr sheets is determined by the length of the R group (Figure 2-4b).<sup>37</sup>

While zirconium phosphates/phosphonates have been studied extensively,<sup>37-39</sup> indium phosphonates have received less attention. Group 13 phosphate/phosphonate chemistry often focuses on Al and those utilizing In are focused on developing cage-like structures.<sup>40-42</sup> We use long aliphatic chains and synthesize the In-phosphonate complexes on a planar support, both of which prevent the formation of cage-like structures. One lamellar In(III) phosphonate found in the literature is  $\text{In}(\text{O}_3\text{PC}_6\text{H}_5)\text{-(O}_2\text{P(OH)C}_6\text{H}_5)\cdot\text{H}_2\text{O}$ .<sup>43</sup> The structure was determined by XRD, TGA, and FTIR. It was determined that the compound exists in sheets similar to other metal phosphonates, and the mix of monoprotonated and deprotonated phosphonate oxygens is consistent with that seen for other trivalent metal phosphonates, including  $\text{Y}^{3+}$ .<sup>4, 43</sup> These similarities to other M(III)-phosphonates lead to the conclusion that InP monolayers will have similar coordination geometries to those in the bulk inorganic species. Another molecular indium phosphonate has been isolated which features an octahedral In center, two waters at the equatorial positions with the phosphate coordinating in the axial positions, and one equivalent of  $\text{ClO}_4^-$  in the unit cell.<sup>40</sup> Zr phosphonates do not incorporate an anion and the addition of one equivalent of  $\text{NO}_3^-$  in our In(III) phosphonate may play a role in the increased thickness of the

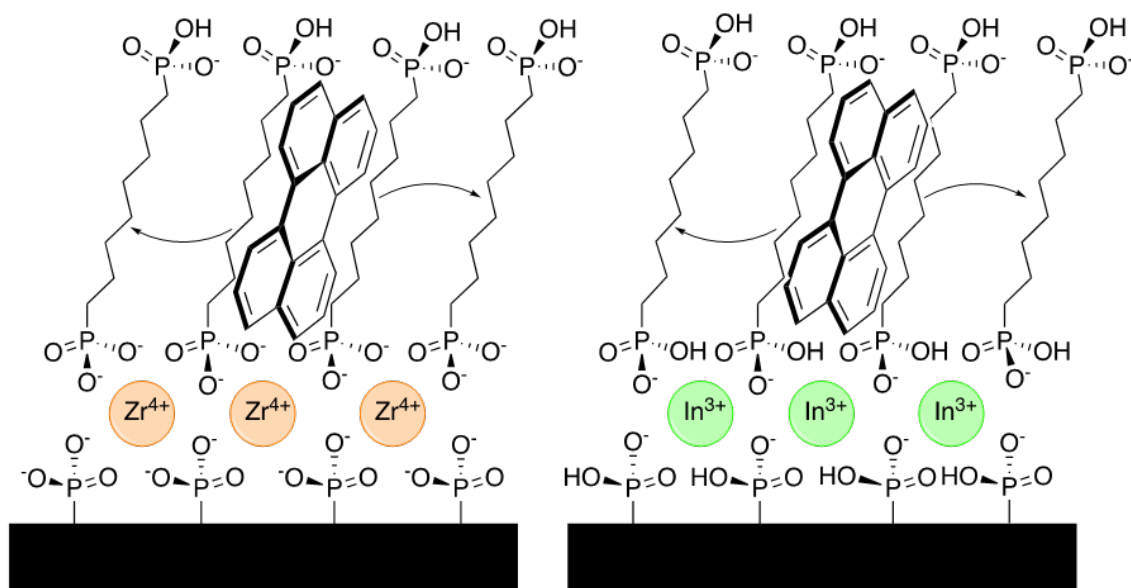
InP adlayer we report here.  $Y^{3+}$  has been reported as used to form metal-bisphosphonate multilayers with  $Zr^{4+}$  and  $Hf^{4+}$ . In this study the multilayer was stable despite the use of a trivalent metal, showing that trivalent metals form layers analogous to tetravalent metals.<sup>4</sup>

*Chromophore diffusion in the monolayer.* Organization within the monolayer is not reflected clearly in the vibrational spectra of the aliphatic chain region. This is because the interchain spacing is determined by the separation between phosphate functionalities on the support surface and does not rely as significantly on interchain interactions as is the case for alkanethiol/Au and other highly organized monolayers.<sup>44-49</sup> An alternative means to evaluate the monolayer properties is to characterize the diffusional behavior of a nonpolar chromophore within the monolayer aliphatic chain region. Rapid diffusion implies significant freedom as a consequence of relatively poor organization of the constituents within the monolayer. Slow diffusion implies restricted motion due to confinement, or at least the absence of void or fluid regions within the monolayer. The quantity of interest is  $D_T$ , the translational diffusion constant, which can be related to the effective viscosity,  $\eta$ , of the medium.

Chromophore translational diffusion is measured using fluorescence recovery after photobleaching (FRAP). FRAP is a well-established technique and there are a number of models available for interpretation of the results. For diffusion in two-dimensional systems, there are three limits in which FRAP data are considered. These are (1) for a chromophore confined within the layer but not chemically bound to layer constituents, (2) for a chromophore bound to the adlayer in some manner where exchange between the bound and unbound state is fast relative to diffusional motion, and (3) for a chromophore bound to the adlayer where the nature of the bonding is either covalent or exhibits exchange kinetics that are slow on the time-scale of

diffusion within the layer. The first order of business is to determine the limiting cases that are appropriate for the experiments we report here.

*Free chromophore diffusion.* For perylene diffusing in a metal phosphonate adlayer (Figure 2-5), there is no bond between the chromophore and the adlayer, so limit (1), or free diffusion applies. We have also synthesized a perylene derivative, BPDI (*vide infra*), that can participate in metal phosphate/phosphonate bonding and the central question is whether the time-scale for site-exchange for the “tethered” chromophore is short or long relative to the time-scale characteristic of diffusion of a free species in the adlayer. If the chromophore exchange rate is slow relative to free chromophore diffusion, then the recovered diffusion constant is



independent of the bleached spot size.<sup>16, 50</sup>

**Figure 2-5. Model of a metal-bisphosphonate monolayer with perylene on a glass substrate.**

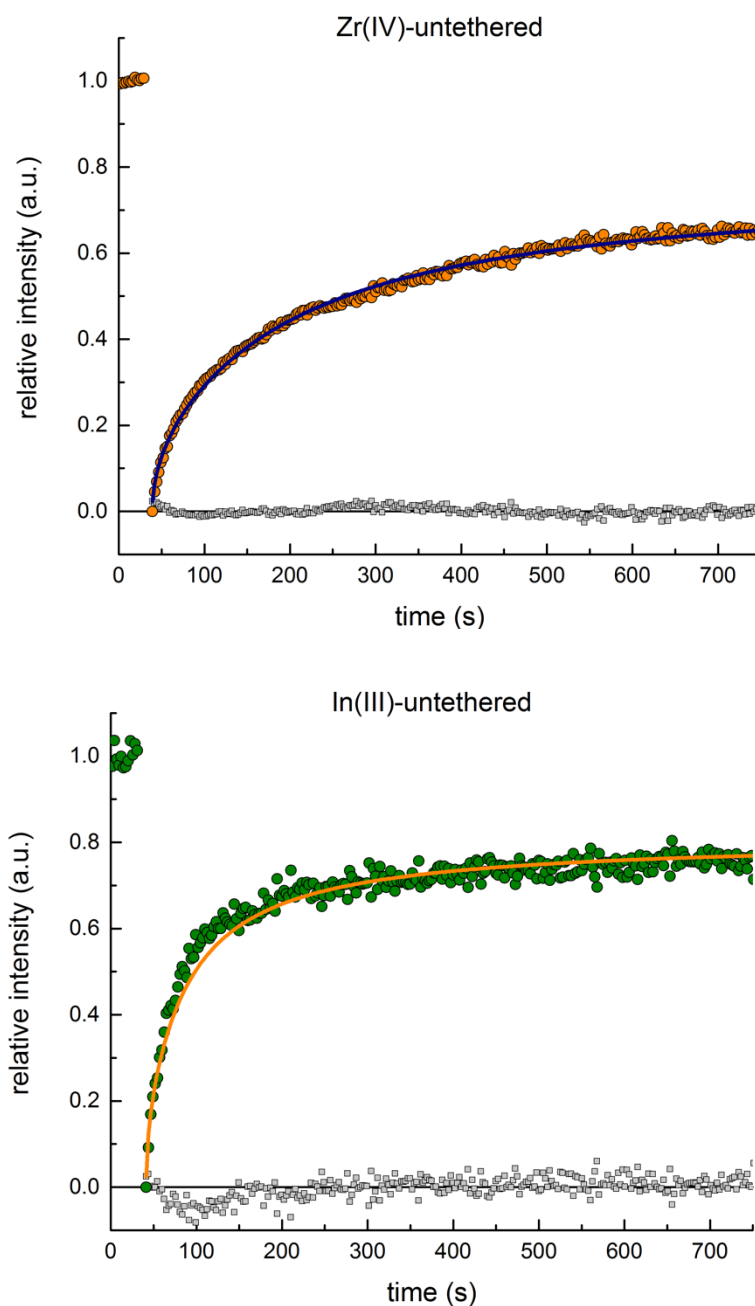


**Figure 2-6. Plot of time (s) vs. relative intensity. These data were obtained from a single FRAP experiment with perylene. Recovery curves do not show 100% recovery due to the photodegradation of the chromophore overtime. Grey squares represent residuals for each recovery curve.**

In order to extract diffusion constant information from our data (Figure 2-6), we apply a double normalization, to account for the photobleaching that is used to characterize the diffusional behavior of the chromophore, and also to account for the slower, overall photobleaching process associated with fluorescence imaging.

$$I_{norm}(t) = \frac{(I_{FRAP}(t) - I_{ref}(t)) \cdot I_{bleach}^{min}}{(I_{pre-FRAP} - I_{pre-ref}) \cdot I_{bleach}^{min}} \quad (1)$$

For each FRAP measurement, two regions are selected, one for the FRAP measurement, and one as a reference region where photobleaching is not performed. The signal components shown in Eq. 1 are as follows.  $I_{norm}(t)$  is the normalized fluorescence recovery after photobleaching signal,  $I_{FRAP}(t)$  and  $I_{ref}(t)$  are the time-dependent fluorescence intensities acquired for the photobleached and reference regions,  $I_{bleach}^{min}$  is the lowest signal intensity in the FRAP measurement,  $I_{bleach}^{min} = I_{FRAP}(0) - I_{ref}(0)$ , and the intensities  $I_{pre-FRAP}$  and  $I_{pre-ref}$  are the fluorescence intensities in the selected regions prior to the photobleaching event.

Raw FRAP data were normalized using Eq. 1. The translational diffusion constant ( $D_T$ ) was found by fitting the normalized FRAP data to Eq. 2a,<sup>50</sup> where  $I_0$  and  $I_1$  are modified Bessel functions of the first kind (Eq. 2b). The resulting fit yields the time constant  $\tau_D$ , which is related to  $D_T$  according to Eq. 3, where  $\omega$  is the radius of the photobleached spot.<sup>16</sup>

$$f(t) = \exp\left(-\frac{2D_T}{\omega^2}t\right) \left[ I_0\left(\frac{2D_T}{\omega^2}t\right) - I_1\left(\frac{2D_T}{\omega^2}t\right) \right] \quad (2a)$$

$$I_\alpha(x) = \frac{1}{\pi} \int_0^\pi e^{x \cos \theta} \cos \alpha \theta d\theta - \frac{\sin \alpha \pi}{\pi} \int_0^\infty e^{-x \cosh t - \alpha t} dt \quad (2b)$$

$$D_T = \frac{\omega^2}{\tau_D} \quad (3)$$

The resulting fits of the normalized experimental data yield values of  $D_T$  shown in Table 1. The results show that  $D_T$  in the Zr-bisphosphonate film is a factor of two slower than it is in the In-bisphosphonate film, and, from these data we can estimate the effective viscosity of the films using the Stokes-Einstein equation,

$$D_T = \frac{k_B T}{6 \pi \eta r} \quad (4)$$

Where  $k_B T$  is the thermal energy ( $T = 293$  K),  $r$  is the radius of the diffusing molecule and  $\eta$  is the viscosity of the medium. The hydrodynamic volume of perylene is  $225 \text{ \AA}^3$ , yielding a value of  $r = 3.8 \text{ \AA}$ . As a comparison, the viscosity of glycerol is *ca.* 1410 cP at room temperature.<sup>51</sup>

**Table 2-1. Translational diffusion constants (DT) for metal-bisphosphonate monolayers with an untethered chromophore (perylene). Viscosity values are determined using Eq. 4.**

Surface	$D_T$ ( $\mu\text{m}^2/\text{s}$ )	$\eta$ (cP)
Zirconium-bisphosphate	$0.31 \pm 0.10$	$1810 \pm 584$
Indium-bisphosphate	$0.63 \pm 0.17$	$895 \pm 242$

These diffusion constant data for the free probe demonstrate that the monolayers both behave effectively as viscous liquids, and there are two potential contributions to this behavior. The first is the intermolecular interactions within the monolayer that serve to impede the diffusional motion of perylene, and the second is the extent to which the association/dissociation equilibrium of the metal bisphosphonate linkage mediates mobility in the monolayer films. These two contributions can be separated to some extent through the use of a tethered chromophore.

*Tethered chromophore diffusion.* To evaluate the contribution of interface association and dissociation dynamics to the properties of the interfaces, we have used a chromophore that is capable of participating in the same equilibrium as the monolayer constituents (Figure 2-2). The tethered chromophore BPDI contains terminal phosphonate functionalities and is similar in length to 1,8-octanedisphosphonic acid, the bisphosphonate used in the metal-bisphosphonate monolayers.<sup>34</sup> The modified perylene chromophore also has a sufficiently high fluorescence quantum yield to be useful for FRAP measurements. We schematize in Figure 2-7 the monolayer structures containing the BPDI chromophore for both ZP and InP linking chemistry. The FRAP data for these monolayers are shown in Figure 2-8, and it is clear that the functional form of the recoveries shown for BPDI is very different than that seen for perylene in the analogous monolayers. This is not a surprising result, and the data for the two chromophores must be treated in the context of related but different models.

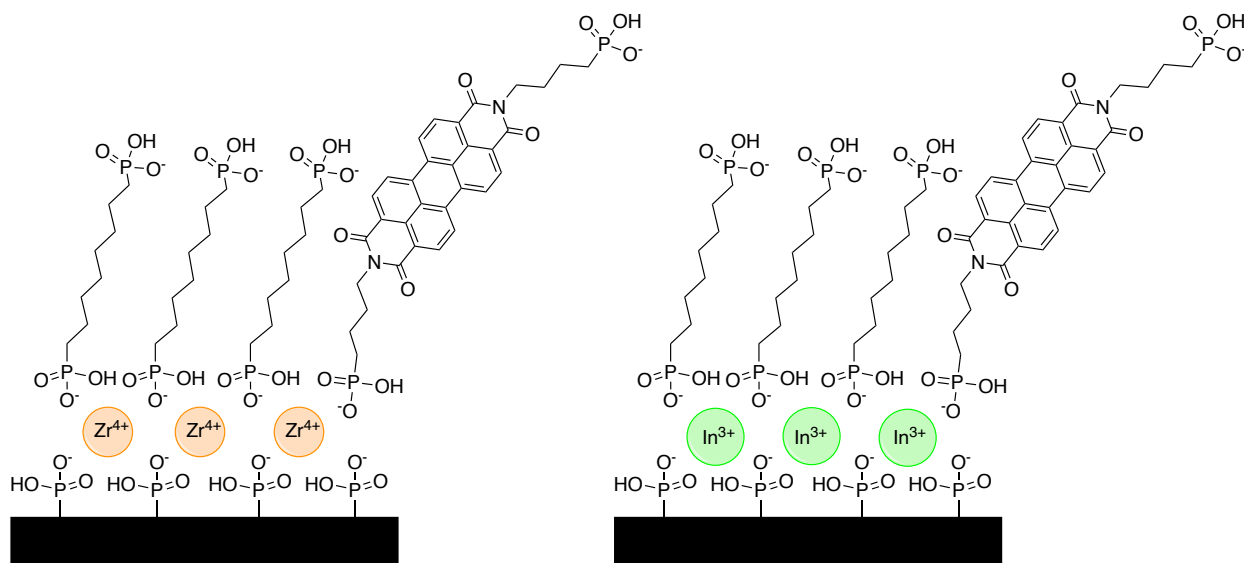


**Figure 2-7. Model of metal-bisphosphonate with BPDI on a glass substrate.**

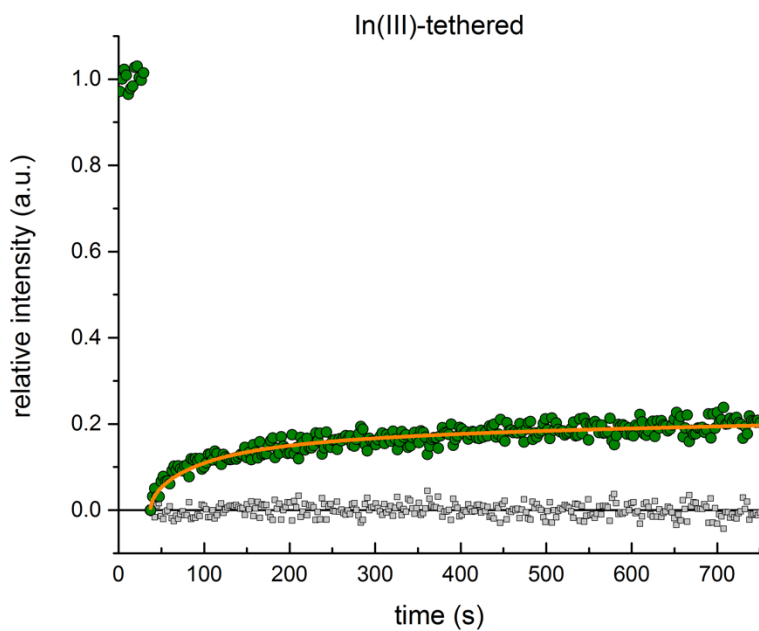
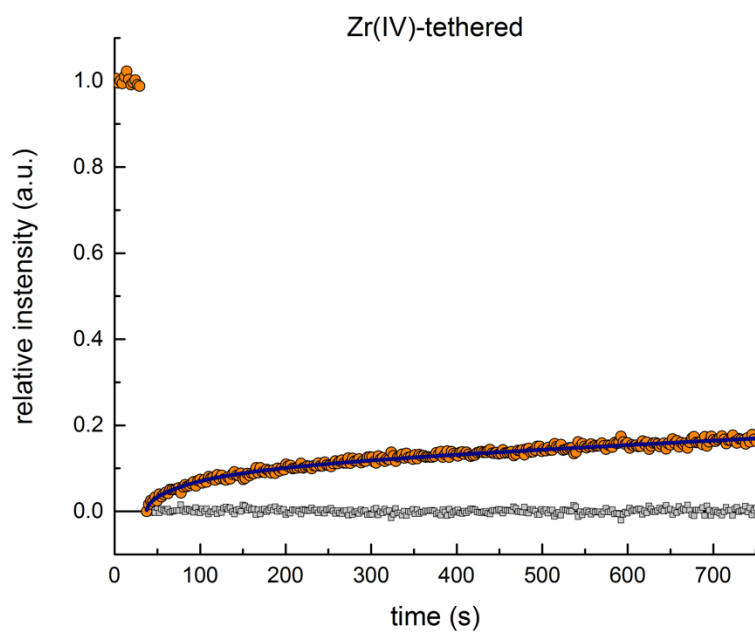


**Figure 2-8. Plot of time (s) vs. relative intensity. This data was obtained from a single FRAP experiment with BPD1. Grey squares represent residuals for each recovery curve.**

The treatment of FRAP data for BPDI requires consideration of the relative rates of interfacial association and dissociation and translational diffusion. If the association and dissociation kinetics are fast relative to the time-scale of molecular motion, then the observed translational diffusion will resemble that seen for the free chromophore. If the association and dissociation kinetics are very slow relative to translational motion, then the FRAP response is observed to be independent of FRAP spot size. Neither of these limiting cases obtain experimentally. The FRAP decay data shown in Figure 2-8 are consistent with contributions from the signal from both translational diffusion and association and dissociation from the interface. Under these conditions, the FRAP decays are modeled using the full reaction-diffusion model (Eq. 4).<sup>52</sup>

$$f(t) = L^{-1} \left[ \frac{1}{p} \frac{F_{eq}}{p} \left( 1 - 2K_1(q) I_1(q) \right) \left( 1 - \frac{k_{on}^*}{p + k_{off}} - \frac{B_{eq}}{p + k_{off}} \right) \right] \quad (4)$$

$$q = \frac{p}{D_i} \left( 1 - \frac{k_{on}^*}{p + k_{off}} \right)^{1/2}$$

$$k_{on}^* = k_{on} m$$

Where  $p$  is the Laplace variable that inverts to yield time,  $L^{-1}$  indicates the inverse Laplace transform of the function contained in brackets,  $\omega$  is the radius of the bleached spot, [m] represents the concentration of available metal ion bonding sites, and the terms  $K_1$  and  $I_1$  are modified Bessel functions. The terms  $F_{eq}$  (equilibrium free concentration) and  $B_{eq}$  (equilibrium bound concentration) are related to  $k_{on}^*$  and  $k_{off}$  by

$$\frac{F_{eq}}{B_{eq}} = \frac{1}{\frac{k_{off}}{k_{on}^* + k_{off}} + \frac{B_{eq}}{k_{on}^* + k_{off}}} \quad (5)$$

Fitting the data in Figure 2-8 to Eq. 4 yield values for  $k_{on}^*$  and  $k_{off}$  shown in Table 2.

**Table 2-2. Translational diffusion constants ( $D_T$ ) for metal-bisphosphonate monolayers with a tethered chromophore, BPDI.**

Surface	$D_T$ $\mu\text{m}^2/\text{s}$	$k_{\text{on}}^*$	$k_{\text{off}}$
Zirconium-bisphosphate	$0.49 \pm 0.22$	$(1.3 \pm 0.4) \times 10^{-4}$	$(8.6 \pm 2.7) \times 10^{-4}$
Indium-bisphosphate	$0.52 \pm 0.11$	$(6.8 \pm 1.4) \times 10^{-5}$	$(2.8 \pm 1.9) \times 10^{-4}$

The values of  $D_T$  for BPDI in the ZP and In-P films are the same to within the experimental uncertainty, but the values of  $k_{\text{on}}^*$  and  $k_{\text{off}}$  are different. This finding is important because it speaks to the similar structural properties of the two films as determined by the overlap in  $D_T$  values, but differences in  $k_{\text{on}}^*$  and  $k_{\text{off}}$  represent a difference in the exchange dynamics. This is not necessarily surprising because in both cases the film density is mediated by the density of phosphate functionality on the support.

It is also important to compare values of  $D_T$  from the free chromophore to those for the bound chromophore. The values are slower by a factor of  $\sim 2$  for the ZP system to  $\sim 3$  for the In-P system. These differences reflect not only the relative importance of equilibrium binding and translational diffusion in determining the properties of these films, but also, they suggest that the surface binding dynamics of the organophosphonates are similar for In and Zr.

## 2.5 Conclusions

While there is significant difference between the ZP and InP monolayers with an untethered chromophore, this difference is not seen for diffusion of a tethered chromophore in the same films. Perhaps of equal significance is the finding that  $D_T$  is of the same magnitude for both free and tethered chromophores. It is possible that in addition to metal phosphonate

binding, the polar upper terminus of the BPDI interacts with the phosphonate functionalities at the top of the monolayer. Such interactions would not be experienced by perylene and may account in part for the similarity of the BPDI  $D_T$  values in the two systems. The main differences between these two surfaces are the charge on the metal ion and, possibly, the packing density.  $\text{In}^{3+}$  has a lower charge and what appears to be a higher packing density, although the details of the packing density may be influenced by the details of the metal ion coordination to the phosphate/phosphonate functionalities. In both cases the films are seen to behave as viscous fluids, as sensed by film constituents. These findings provide useful insight into the potential utility of metal-phosphonate monolayers and similar films.

## **APPENDIX**

## Appendix

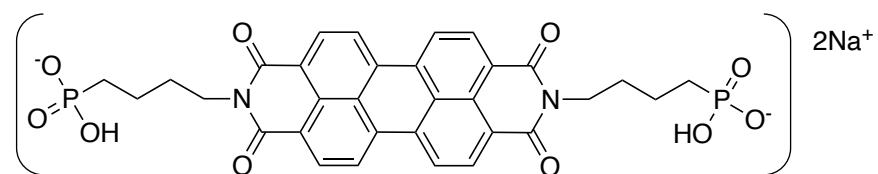


Figure A2-1. Structure of tethered chromophore BDPI.

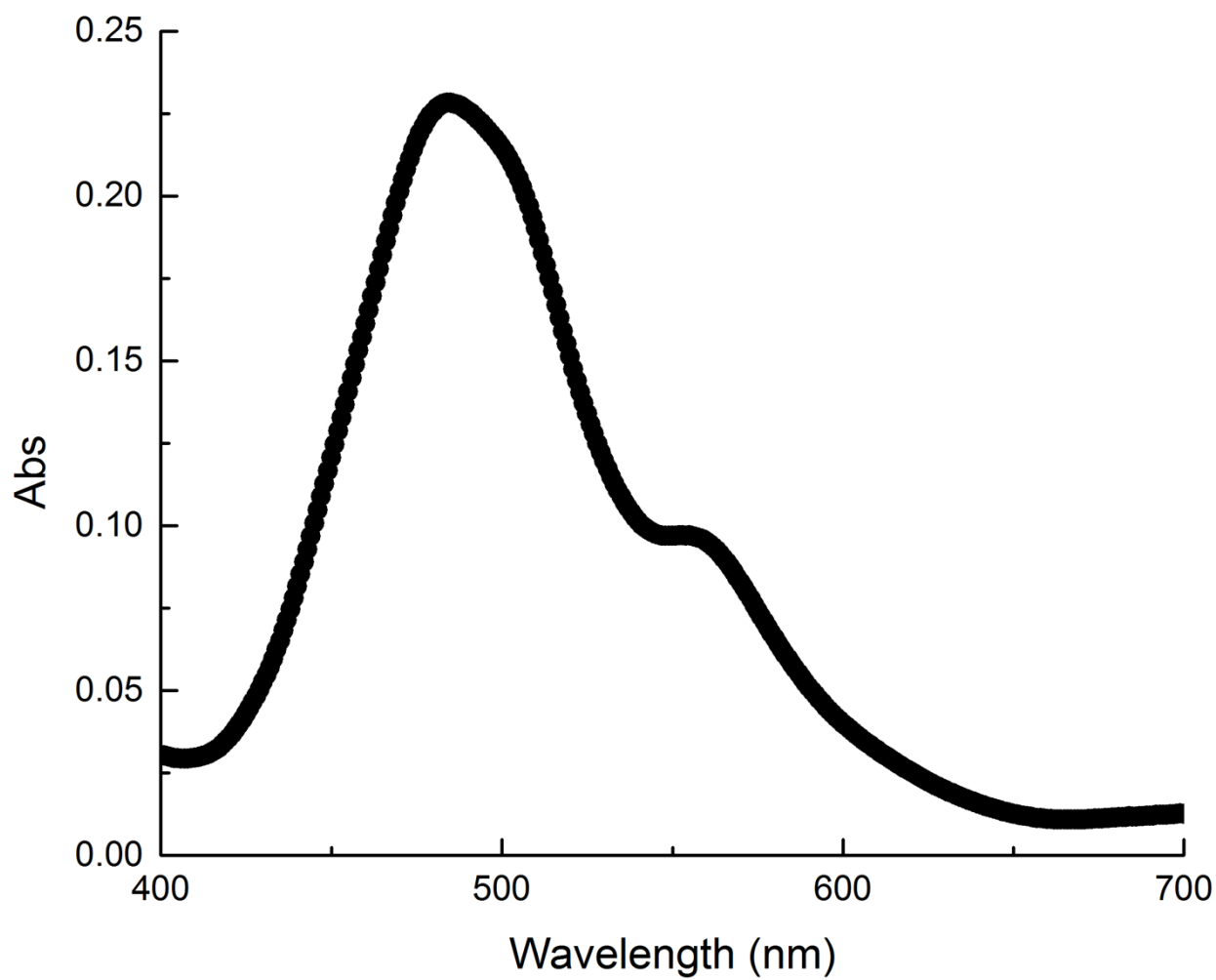
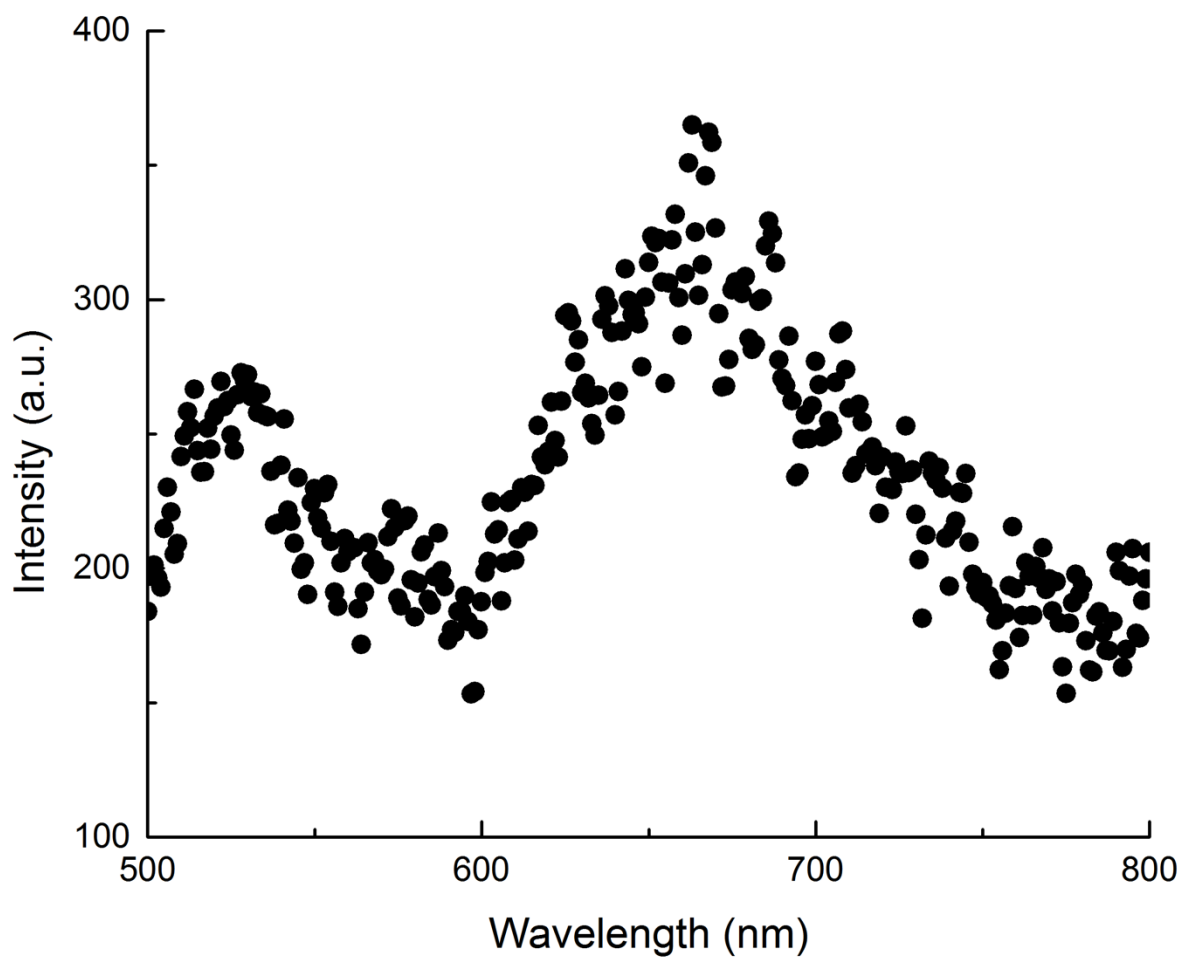


Figure A2-2. Absorption spectrum of BDPI.  $\lambda_{\text{max}}$ :484nm



**Figure A2-3. Emission spectrum of BDPI.  $\lambda_{\text{max}}$ : 668nm**

## **REFERENCES**

## REFERENCES

1. Dubois, L. H.; Nuzzo, R. G., Synthesis, Structure, and Properties of Model Organic-Surfaces. *Annu. Rev. Phys. Chem.* **1992**, *43*, 437-463.
2. Ulman, A., Formation and structure of self-assembled monolayers. *Chem Rev* **1996**, *96* (4), 1533-1554.
3. Han, X. M. Y.; Sun, S. Q.; He, T., Preparation and photolithography of self-assembled monolayers of 10-mercaptodecanylphosphonic acid on glass mediated by zirconium for protein patterning. *Colloid Surface B* **2013**, *108*, 66-71.
4. Love, J. C.; Estroff, L. A.; Kriebel, J. K.; Nuzzo, R. G.; Whitesides, G. M., Self-assembled monolayers of thiolates on metals as a form of nanotechnology. *Chem Rev* **2005**, *105* (4), 1103-1169.
5. Schreiber, F., Structure and growth of self-assembling monolayers. *Prog Surf Sci* **2000**, *65* (5-8), 151-256.
6. Ishida, T.; Terada, K.; Hasegawa, K.; Kuwahata, H.; Kusama, K.; Sato, R.; Nakano, M.; Naitoh, Y.; Haga, M., Self-assembled monolayer and multilayer formation using redox-active Ru complex with phosphonic acids on silicon oxide surface. *Appl Surf Sci* **2009**, *255* (21), 8824-8830.
7. Blodgett, K. B., Films Built by Depositing Successive Monomolecular Layers on a Solid Surface. *J Am Chem Soc* **1935**, *57* (6), 1007-1022.
8. Cao, G.; Hong, H. G.; Mallouk, T. E., Layered Metal Phosphates and Phosphonates - from Crystals to Monolayers. *Accounts of Chemical Research* **1992**, *25* (9), 420-427.
9. Cao, G.; Lynch, V. M.; Swinnea, J. S.; Mallouk, T. E., Synthesis and Structural Characterization of Layered Calcium and Lanthanide Phosphonate Salts. *Inorg Chem* **1990**, *29* (11), 2112-2117.
10. Horne, J. C.; Blanchard, G. J., Dynamics within a single molecular layer. Aggregation, relaxation, and the absence of motion. *J Am Chem Soc* **1996**, *118* (50), 12788-12795.
11. Lee, H.; Kepley, L. J.; Hong, H. G.; Akhter, S.; Mallouk, T. E., Adsorption of Ordered Zirconium Phosphonate Multilayer Films on Silicon and Gold Surfaces. *J Phys Chem-US* **1988**, *92* (9), 2597-2601.
12. Neff, G. A.; Page, C. J.; Meintjes, E.; Tsuda, T.; Pilgrim, W. C.; Roberts, N.; Warren, W. W., Hydrolysis of surface-bound phosphonate esters for the self-assembly of multilayer films: Use of solid state magic angle spinning P-31 NMR as a probe of reactions on surfaces. *Langmuir* **1996**, *12*, 238-242.

13. Thompson, M. E., Use of Layered Metal Phosphonates for the Design and Construction of Molecular Materials. *Chemistry of Materials* **1994**, *6* (8), 1168-1175.
14. Yang, H. C.; Aoki, K.; Hong, H. G.; Sackett, D. D.; Arendt, M. F.; Yau, S. L.; Bell, C. M.; Mallouk, T. E., Growth and Characterization of Metal(Ii) Alkanebisphosphonate Multilayer Thin-Films on Gold Surfaces. *J Am Chem Soc* **1993**, *115* (25), 11855-11862.
15. Yang, X.; Zhao, H.; Gao, S. Y., Layer-by-Layer Self-Assembly of Pd Films and Their Catalytic Properties toward Nitroarenes Hydrogenation. *Ind Eng Chem Res* **2017**, *56* (12), 3429-3435.
16. Baumler, S. M.; Reidy, T. M.; Blanchard, G. J., Diffusional motion as a gauge of fluidity and interfacial adhesion. Supported alkylphosphonate monolayers. *J Colloid Interf Sci* **2016**, *468*, 145-155.
17. O'Brien, J. T.; Zeppenfeld, A. C.; Richmond, G. L.; Page, C. J., Fourier-Transform Infrared-Spectroscopy Studies of Hafnium Alkylbis(Phosphonate) Multilayers On Gold - Effects of Alkylbis(Phosphonate) Chain-Length, Substrate Roughness, and Surface Functionalization On Film Structure and Order. *Langmuir* **1994**, *10*, 4657-4663.
18. Zeppenfeld, A. C.; Fiddler, S. L.; Ham, W. K.; Klopfenstein, B. J.; Page, C. J., Variation of Layer Spacing in Self-Assembled Hafnium-1,10- Decanediybis(Phosphonate) Multilayers As Determined By Ellipsometry and Grazing Angle X-Ray-Diffraction. *J. Am. Chem. Soc.* **1994**, *116*, 9158-9165.
19. Neff, G. A.; Helfrich, M. R.; Clifton, M. C.; Page, C. J., Layer-by-layer growth of acentric multilayers of Zr and azobenzene bis(phosphonate): Structure, composition, and second-order nonlinear optical properties. *Chemistry of Materials* **2000**, *12* (8), 2363-2371.
20. Bent, S. F.; Schilling, M. L.; Wilson, W. L.; Katz, H. E.; Harris, A. L., Structural Characterization of Self-Assembled Multilayers by Ftir. *Chemistry of Materials* **1994**, *6* (2), 122-126.
21. Kohli, P.; Blanchard, G. J., Probing interfaces and surface reactions of zirconium phosphate/phosphonate multilayers using P-31 NMR spectrometry. *Langmuir* **2000**, *16* (2), 695-701.
22. Marcon, R. O.; Brochsztain, S., Characterization of self-assembled thin films of zirconium phosphonate/aromatic diimides. *Thin Solid Films* **2005**, *492* (1-2), 30-34.
23. Shannon, R. D., Revised Effective Ionic-Radii and Systematic Studies of Interatomic Distances in Halides and Chalcogenides. *Acta Crystallogr A* **1976**, *32* (Sep1), 751-767.
24. Mooney, R. C. L., Crystal Structure of Anhydrous Indium Phosphate and Thallic Phosphate by X-Ray Diffraction. *Acta Crystallogr* **1956**, *9* (2), 113-117.

25. Alberti, G.; Costantino, U.; Allulli, S.; Tomassini, N., Crystalline  $Zr(R-PO_3)_2$  and  $Zr(R-OPO_3)_2$  Compounds (R=Organic Radical) - New Class of Materials Having Layered Structure of Zirconium-Phosphate Type. *J Inorg Nucl Chem* **1978**, *40* (6), 1113-1117.
26. Clearfield, A., Chapter 1 The Early History and Growth of Metal Phosphonate Chemistry. In *Metal Phosphonate Chemistry: From Synthesis to Applications*, The Royal Society of Chemistry: 2012; pp 1-44.
27. Clearfield, A.; Duax, W. L., Crystal Structure of Ion Exchanger Zirconium Bis(Monohydrogen Orthoarsenate) Monohydrate. *Acta Crystall B-Stru* **1969**, *B 25*, 2658-+.
28. Richards, A. F.; Beavers, C. M., Synthesis and structures of a pentanuclear Al(III) phosphonate cage, an In(III) phosphonate polymer, and coordination compounds of the corresponding phosphonate ester with  $GaI_3$  and  $InCl_3$ . *Dalton T* **2012**, *41* (37), 11305-11310.
29. Goura, J.; Chandrasekhar, V., Molecular Metal Phosphonates. *Chem Rev* **2015**, *115* (14), 6854-6965.
30. Chandrasekhar, V.; Goura, J.; Duthie, A., Molecular Indium(III) Phosphonates Possessing Ring and Cage Structures. Synthesis and Structural Characterization of  $[In_2(t-BuPO_3H)_4(phen)_2Cl_2]$  and  $[In_3(C_5H_9PO_3)_2(C_5H_9PO_3H)_4(phen)_3] \cdot NO_3 \cdot 3.5H_2O$ . *Inorg Chem* **2013**, *52* (9), 4819-4824.
31. Morizzi, J.; Hobday, M.; Rix, C., Synthesis and characterisation of some lamellar indium phosphonates. *J Mater Chem* **1999**, *9* (4), 863-864.
32. Akhter, S.; Lee, H.; Hong, H. G.; Mallouk, T. E.; White, J. M., Structural characterization of multilayer metal phosphonate film on silicon using angular-dependent x-ray photoelectron spectroscopy. *Journal of Vacuum Science & Technology A* **1989**, *7* (3), 1608-1613.
33. Allara, D. L.; Nuzzo, R. G., Spontaneously Organized Molecular Assemblies .2. Quantitative Infrared Spectroscopic Determination of Equilibrium Structures of Solution-Adsorbed Normal-Alkanoic Acids On an Oxidized Aluminum Surface. *Langmuir* **1985**, *1*, 52-66.
34. Allara, D. L.; Swalen, J. D., An Infrared Reflection Spectroscopy Study of Oriented Cadmium Arachidate Monolayer Films On Evaporated Silver. *J. Phys. Chem.* **1982**, *86*, 2700-2704.
35. Evans, S. D.; Goppertberarducci, K. E.; Urankar, E.; Gerenser, L. J.; Ulman, A., Monolayers Having Large Inplane Dipole-Moments - Characterization of Sulfone-Containing Self-Assembled Monolayers of Alkanethiols On Gold By Fourier-Transform Infrared-Spectroscopy, X-Ray Photoelectron-Spectroscopy, and Wetting. *Langmuir* **1991**, *7*, 2700-2709.
36. Porter, M. D.; Bright, T. B.; Allara, D. L.; Chidsey, C. E. D., Spontaneously Organized Molecular Assemblies .4. Structural Characterization of Normal-Alkyl Thiol Monolayers On Gold By Optical Ellipsometry, Infrared-Spectroscopy, and Electrochemistry. *J. Am. Chem. Soc.* **1987**, *109*, 3559-3568.

37. Smith, E. L.; Porter, M. D., Structure of Monolayers of Short-Chain N-Alkanoic Acids ( $\text{CH}_3(\text{CH}_2)_n\text{COOH}$ ,  $n = 0-9$ ) Spontaneously Adsorbed From the Gas- Phase At Silver As Probed By Infrared Reflection Spectroscopy. *J. Phys. Chem.* **1993**, *97*, 8032-8038.
38. Stole, S. M.; Porter, M. D., Insitu Infrared External Reflection Spectroscopy As a Probe of the Interactions At the Liquid Solid Interface of Long-Chain Alkanethiol Monolayers At Gold. *Langmuir* **1990**, *6*, 1199-1202.
39. Soumpasis, D. M., Theoretical-Analysis of Fluorescence Photobleaching Recovery Experiments. *Biophys J* **1983**, *41* (1), 95-97.
40. Segur, J. B.; Oberstar, H. E., Viscosity of Glycerol and Its Aqueous Solutions. *Ind Eng Chem* **1951**, *43* (9), 2117-2120.
41. Sprague, B. L.; Pego, R. L.; Stavreva, D. A.; McNally, J. G., Analysis of Binding Reactions by Fluorescence Recovery after Photobleaching *Biophys. J.* **2004**, *86*, 3473-3495.

## **Chapter Three: Translational Diffusion Dynamics in Divalent Metal Phosphonate Monolayers**

### **3.1 Abstract**

Self-assembled monolayers are attractive for surface modification due to their ease of synthesis and the range of chemical functionality that can be applied. Metal-phosphonate monolayer properties can be controlled through the metal ions that can be used in their formation. The organization and fluid properties of these monolayers can be understood in the context of their thermodynamic properties and the association and dissociation kinetics that proceed at the metal-phosphonate complex. In this work four different M(II)-phosphonate monolayers were synthesized, and the diffusional behavior of free and tethered chromophores was evaluated using fluorescence recovery after photobleaching (FRAP) measurements.

### **3.2 Introduction**

Mono- and multilayer molecular films have been studied extensively because of their potential utility in a range of applications and because they are a useful structural motif for the study of fundamental processes in a quasi two-dimensional format. Using such structures, it is possible to modify interfacial properties, such as polarity or chemical reactivity, significantly. Applications such as lubrication (tribology) and chemical sensing have been the beneficiaries of fundamental developments in interfacial mono- and multilayer systems.<sup>18, 20, 21, 53, 54</sup> Interfacial monolayers can be classified based on the nature of their interaction(s) with the support on which they are deposited. Langmuir-Blodgett monolayers are typically physisorbed to the support and alkanethiol-coinage metal interfaces are chemically bonded, with the strength of the bond being somewhat less than a typical covalent bond. Modification of surfaces using siloxane bonding produces fully covalently bonded structures,<sup>12, 55-60</sup> and metal-bisphosphonate interfaces rely on metal ion complexation chemistry to form. This latter group of materials has proven to be of particular interest because of their relative ease of formation and the ability to control the

monolayer-support interactions through the identity of the metal ion used. Zr(IV) and Hf(IV) bisphosphonate films have been studied extensively because of the thermodynamics of the resulting metal bisphosphonate complex.<sup>6, 23, 24, 61-68</sup> Free energies of formation for these tetravalent metal complexes are in excess of -60 kcal/mol.<sup>69</sup> Divalent metal ions have also been studied, including Co(II), Ca(II), Mg(II), Ni(II), Zn(II), and Mn(II).<sup>23, 27</sup> Not surprisingly, the resulting metal bisphosphonate films are bound less strongly than those formed using tetravalent metal ions, resulting in useful physical properties for certain applications.

We are interested in controlling the fluid properties of interfacial mono- and multilayer structures. As noted above, the two limits of monolayer fluidity are well established; Langmuir Blodgett monolayers are physisorbed and consequently the monolayer constituents are expected to exhibit translational mobility. In contrast, covalently bound adlayers do not exhibit translational freedom. Using metal ion complexation is attractive as a means of monolayer bonding because it is an equilibrium process and, in addition to dissociation and diffusion, there is the opportunity to control the free energy of bonding and potentially the translational freedom of monolayer constituents. The examination of constituent freedom in monolayers is best accomplished through the direct measurement of translational diffusion of monolayer constituents and moieties incorporated into but not bonded to the monolayer.<sup>16</sup>

Here the translational dynamics of MP monolayers featuring a 2<sup>+</sup> metal ion are reported. Co(II), Ca(II), Mg(II), and Ni(II) were used. These four MP monolayers have been previously described and feature a mix of group II and transition metals. Using more than one divalent metal allows for the determination of the effect of metal identity on the surface fluidity as well as decreasing the charge. The translational dynamics will be compared to ZP and indium bisphosphonate (InP) monolayers there were previously described to determine the effect of

metal ion charge on these systems. Changing the metal can result in a number of different surface changes including a change in the metal ion complexation dynamics between the metal and the phosphonate groups, but also a change in packing density and film organization, all of which could impact the translational dynamics of the monolayer constituents.

Fluorescence recovery after photobleaching (FRAP) is the technique that was used to measure translational diffusion in the systems we consider here. Metal ion-dependent variation in the diffusional behavior of monolayers provides insight into the kinetics of metal bisphosphonate dissociation and the diffusion of chromophores not tethered to the monolayer provides insight into organization within the monolayer. Both are described here with four different MP monolayers formed using divalent metal ions.

### 3.3 Experimental

*Chemicals used:* Concentrated sulfuric acid, 2,4,6-collidine,  $\text{CaCl}_2$ ,  $\text{CoCl}_2 \cdot 6\text{H}_2\text{O}$ ,  $\text{NiCl}_2 \cdot 6\text{H}_2\text{O}$ , octanoyl chloride,  $\text{POCl}_3$ , perylene, and 1,8-octanebisphosphonic acid were obtained from Sigma-Aldrich in their highest purity forms and used without further purification.  $\text{MgCl}_2 \cdot 6\text{H}_2\text{O}$  (99%) was obtained from CCI Chemical and used without further purification. All water was purified using a Milli-Q purification system.  $\text{N,N}'$ -bis(4-phosphonobutyl)-3,4,9,10-perylenediimide (BPDI) was synthesized as previously described.<sup>70</sup>

*Metal bisphosphonate monolayer synthesis.* Piranha solution (*Caution! Strong oxidizer!*) was used to clean glass or oxidized silicon plates (1cm x 1cm) that were used as monolayer supports. Plates were immersed in piranha solution for 15 minutes. The plates were then rinsed with 18 M $\Omega$  water and immersed in a 2M HCl solution for 5 minutes. The plates were rinsed with 18 M $\Omega$  water and then with anhydrous acetonitrile. The surface was immediately phosphorylated by immersion in 100 mM  $\text{POCl}_3$  and 100 mM 2,4,6-collidine in dry acetonitrile

for one hour, then rinsed with anhydrous acetonitrile. The plates were then treated overnight with 5 mM metal ion solution,  $\text{CaCl}_2$ ,  $\text{CoCl}_2 \cdot 6\text{H}_2\text{O}$ ,  $\text{NiCl}_2 \cdot 6\text{H}_2\text{O}$ ,  $\text{MgCl}_2 \cdot 6\text{H}_2\text{O}$ ,  $\text{ZrOCl}_2$ , or  $\text{In}(\text{NO}_3)_3 \cdot \text{x H}_2\text{O}$ .<sup>7, 35</sup> For reasons of solubility, 100% ethanol was used as the solvent for all solutions using  $\text{M}^{2+}$  salts and a 60% EtOH/ 40%  $\text{H}_2\text{O}$  solvent mixture was used for Zr(IV) and In(III).<sup>27</sup> After washing with Milli-Q water, the plates were treated with 1.25 mM 1,8-octanebisphosphonic acid in ethanol for one hour. The pH of all metal ion-containing and phosphonate-containing solutions was maintained between 2 and 4 using dilute HCl to minimize the formation of metal hydroxides. For substrates used to perform FRAP measurements, the phosphonate solution contained 1 mol% of the chromophore (*vide infra*, Figure 3-1).

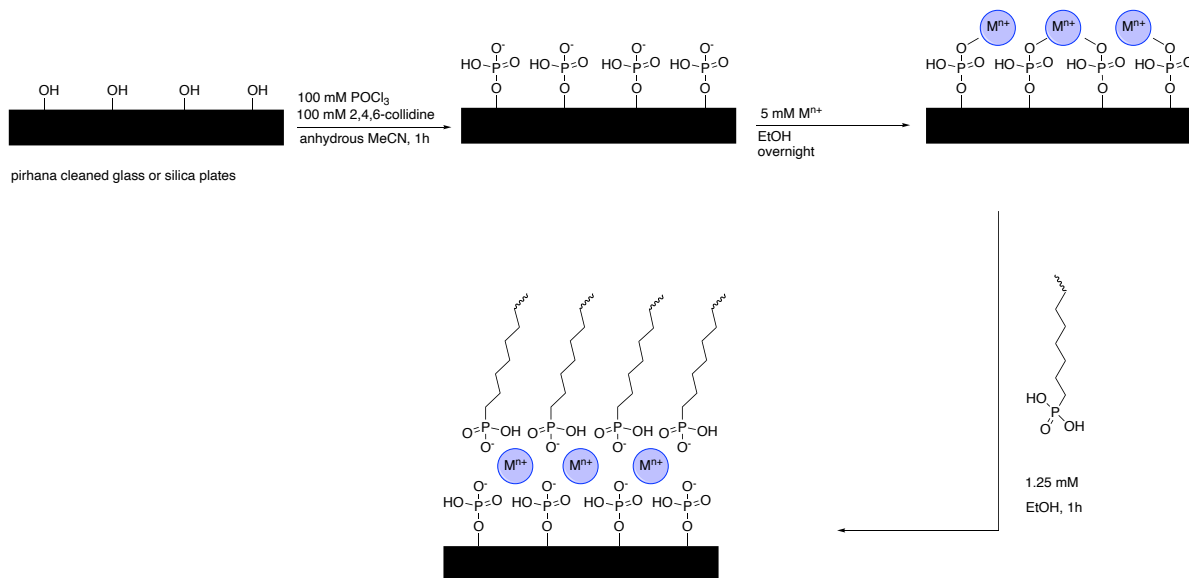
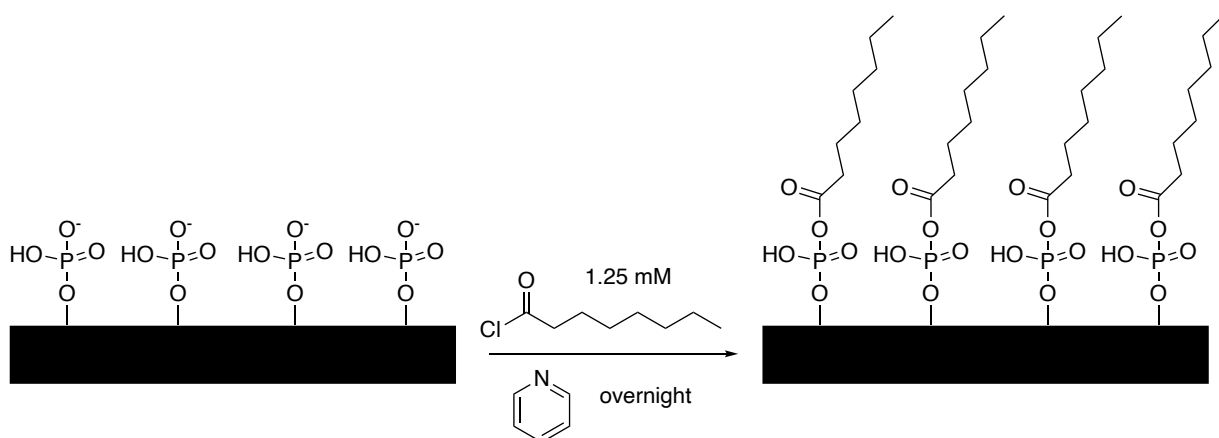


**Figure 3-1. Schematic of MP monolayer synthesis.**

*Covalent phosphonate monolayer synthesis.* As a control, a monolayer was formed by covalent bonding rather than metal ion complexation. This monolayer was prepared as described above to functionalize the support surface with phosphates. The resulting surface was then treated with 1.25 mM octanoyl chloride in pyridine overnight to produce the monolayer shown in Figure



3-2.

**Figure 3-2. Schematic of phosphonate monolayer synthesis.**

*Optical ellipsometry.* A spectroscopic ellipsometer (Gaertner) equipped with a 75 W xenon lamp source and an M-44 detector with an EC110 multiwavelength control module was used to determine film thickness. All thickness measurements were performed on silicon supports cleaned with piranha solution ( $1\text{H}_2\text{O}_2:3\text{HNO}_3$ ). This preparation method produces a *ca.* 15 Å oxide film which can be phosphorylated and reacted to produce the monolayers described above. A minimum of ten spots across each substrate were measured and the reported values are the averages (and standard deviations) of these measurements.

*Fluorescence Recovery After Photobleaching (FRAP).* A Nikon C2+ confocal laser scanning microscopy system with a Nikon Eclipse Ti-E inverted microscope with a confocal

scanning system (Nikon Ti-S-CON) was utilized for acquiring FRAP data. A 20× objective lens was used for all experiments. The chromophores were excited at 488 nm with a diode laser (Nikon Lu-N4) and detected using a PMT detector system (Nikon C2-DU3, 400nm-700nm). For perylene the 405 nm diode laser was used for excitation and for BPDI, the 488 nm diode laser was used. For both the tethered (BPDI) and untethered (perylene) systems, initial intensity was measured for 30 sec, bleached for 5 sec, and recovery was monitored for a minimum of 3 minutes for the untethered systems a minimum of 12 minutes for systems with a tethered chromophore. A minimum of ten spots across each monolayer were measured in this manner.

### **3.4 Results and Discussion**

In this work we focus on the use of divalent metal ions rather than tri- and quadrivalent metal ions. Our interest in the use of divalent metal ions stems from the comparatively weak bisphosphonate complexes formed. The equilibrium constant for these complexes is the ratio of the association rate constant and the dissociation rate constant. Depending on which of these rate constants is the dominant cause of change in the equilibrium constant, we may observe either a significant change or not in the diffusional behavior of the tethered chromophore BPDI. Similarly, we anticipate that the organization and intermolecular interactions of the monolayer constituents will determine the diffusional behavior of the free chromophore perylene. Taken collectively, these data will provide insight into the structural and compositional factors that influence monolayer properties to the greatest extent and will guide subsequent developments for specific applications.

The diffusional dynamics of In(III)-bisphosphonate and Zr(IV)-bisphosphonate monolayers have been reported previously.<sup>11</sup> In that work, we found that the dynamics of tethered chromophores are similar for the two metal-bisphosphonate monolayers, suggesting that

the metal-phosphonate dissociation constant is mediating diffusional motion. While the diffusion constant for the tethered chromophore was similar, the diffusion constant for the free probe differed significantly for monolayers formed with the two metal ions. We have chosen to use divalent metals to determine whether metal-phosphonate dissociation is likewise limiting for these monolayers. We have selected Mg(II), Ca(II), Co(II), and Ni(II) for this work. Metal-phosphonate monolayers have been reported before previously for each of these metal ions, and the use of group II metals and transition metals allows for a broad comparison to be made.

Optical ellipsometry is a useful method to determine the thickness of the MP monolayers and, simultaneously to verify that they have been formed on the support surface. For all of the monolayers examined here we expect a thickness of *ca.* 20 Å based on molecular mechanics calculations of the species used in monolayer formation (23 Å) and a non-zero tilt angle with respect to the support surface normal. The ionic radii of Mg, Ca, Co, and Ni are sufficiently close to one another that ellipsometric thicknesses are not expected to depend on the identity of the metal ion used.<sup>35</sup> The experimental results are shown in Table 3-4-1. We note that the observation of a thickness consistent with a single monolayer is not proof of uniform monolayer coverage but does rule out the presence of extensive multilayer formation or substantially sub-monolayer coverage. To evaluate the long-term stability of the formed monolayers, ellipsometric measurements were taken after samples of each of the films was immersed in DI water for *ca.* 96h. In all cases there was no change in the ellipsometric thickness exceeding the experimental uncertainty (Table 3-1).

**Table 3-1. Thickness measurements from ellipsometric measurements.**

Surface	thickness (Å)	Ionic radius of M(II) (Å) <sup>35</sup>	thickness after 96h in H <sub>2</sub> O (Å)
Ni(II)- O <sub>3</sub> P-C <sub>8</sub> H <sub>16</sub> -PO <sub>3</sub> H	19 ± 1	0.55	20 ± 1
Mg(II)- O <sub>3</sub> P-C <sub>8</sub> H <sub>16</sub> -PO <sub>3</sub> H	20 ± 1	0.57	20 ± 1
Co(II)- O <sub>3</sub> P-C <sub>8</sub> H <sub>16</sub> -PO <sub>3</sub> H	20 ± 1	0.78	20 ± 1
Ca(II)- O <sub>3</sub> P-C <sub>8</sub> H <sub>16</sub> -PO <sub>3</sub> H	20 ± 1	1.00	20 ± 1

While the focus of this study is on metal-phosphonate monolayers, analogous metal-phosphonate inorganic compounds have been studied and the coordination geometries of the bulk species have been shown to correspond to that seen in MP monolayers.<sup>bv</sup> The literature shows that MP films exhibit at 1:2 metal-to-phosphonate ratio,<sup>10, 11</sup> regardless of the formal charge on the metal ion (II, III, or IV). Incorporation of counterions and protonation of the phosphate or phosphonate group(s) is required for macroscopic charge neutrality.<sup>11</sup>

*Chromophore diffusion in M(II)-bisphosphonate monolayers.* To evaluate the extent of organization within the MP monolayer, we measure the translational diffusion of a chromophore within the aliphatic region of the M(II)P films. The translational diffusion constant,  $D_T$ , is measured for chromophores in the M(II)P films using FRAP, and  $D_T$  is related to the effective viscosity of the monolayer through the Stokes-Einstein relation. A comparatively large value of  $D_T$  implies a low viscosity, which corresponds to a low degree of intermolecular order or organization within the monolayer. Conversely, small  $D_T$  values imply a relatively high viscosity within the monolayer, a condition associated with strong intermolecular constituent interactions and potential order within the monolayer.

FRAP is a widely used technique to characterize diffusion in thin films and other comparatively confined quasi-2D systems, such as plasma membranes.<sup>71</sup> Because of the range of systems that have been studied by FRAP, there are a number of different models extant for the extraction of information from the data. In this work we utilize the well-established Soumpasis model<sup>50</sup> in two limits for the characterization of free and tethered chromophores in the monolayers we consider. For free chromophore diffusion, the diffusing species is not chemically bonded to the monolayer but is confined within the nonpolar aliphatic region of the monolayer. For tethered diffusion the chromophore is functionalized such that becomes a structural component of the monolayer, bound by the same metal ion complexation that is responsible for the formation of the monolayer.<sup>16, 50</sup> We consider these two systems separately.

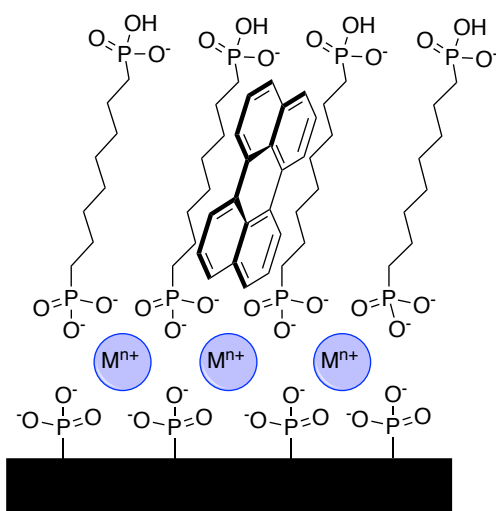


**Figure 3-3. Perylene incorporated in a MP monolayer. The protonation of the oxygens involved in metal binding depends on charge balance and for the sake of clarity are shown unprotonated here.**

*Free chromophore diffusion.* For these experiments we use the chromophore perylene (Figure 3-3). The choice of perylene is driven by the fact that it is insoluble in water but incorporates readily into the nonpolar aliphatic chain region of the monolayers we consider here. Perylene is not chemically bonded to any constituent within the monolayer and can diffuse freely

within the aliphatic chain region. FRAP data exhibit rapid photobleaching of selected regions when exposed to intense radiation, and comparatively slow photobleaching of the chromophore under conditions of low intensity irradiation used for purposes of observation. Because both phenomena contribute to the overall FRAP signal, the raw time-dependent intensity data are normalized according to Eq. 1. Data treated in this manner are shown in Figure 3-4.

$$I_{norm}(t) = \frac{I_{FRAP}(t) - I_{ref}(t) - I_{bleach}^{min}}{I_{pre-FRAP} - I_{pre-ref} - I_{bleach}^{min}} \quad (1)$$

The FRAP measurement consists of selecting two regions of the same size, one of which is photobleached and the other which serves as a reference region. The quantities in Eq. 1 are defined as follows.  $I_{norm}(t)$  is the normalized fluorescence recovery after photobleaching signal,  $I_{FRAP}(t)$  and  $I_{ref}(t)$  are the time-dependent fluorescence intensities acquired for the photobleached and reference regions, respectively,  $I_{bleach}^{min}$  is the lowest signal intensity in the FRAP measurement,  $I_{bleach}^{min} = I_{FRAP}(0) - I_{ref}(0)$ , and the intensities  $I_{pre-FRAP}$  and  $I_{pre-ref}$  are the fluorescence intensities in the selected regions prior to the photobleaching event. The functional form of the normalized recovery signal is given by Eq. 2 and is determined by the intermolecular interactions that mediate chromophore diffusion within the monolayer.

$$I_{norm}(t) = \exp\left(-\frac{2D}{D_T}t\right) \left[ I_0 \frac{2D}{D_T}t - I_1 \frac{2D}{D_T}t \right] \quad (2)$$

The quantity of interest is the translational diffusion constant ( $D_T$ ), which is extracted from the data by fitting the experimental  $I_{norm}(t)$  data to Eq. 2.<sup>50</sup> In Eq. 2, the terms  $I_0$  and  $I_1$  are modified Bessel functions of the first kind and the term  $\tau_D$  is related to  $D_T$  and the radius of the photobleached region (Eq. 3),<sup>16</sup>

$$D = \frac{2}{\tau_D} \quad (3)$$

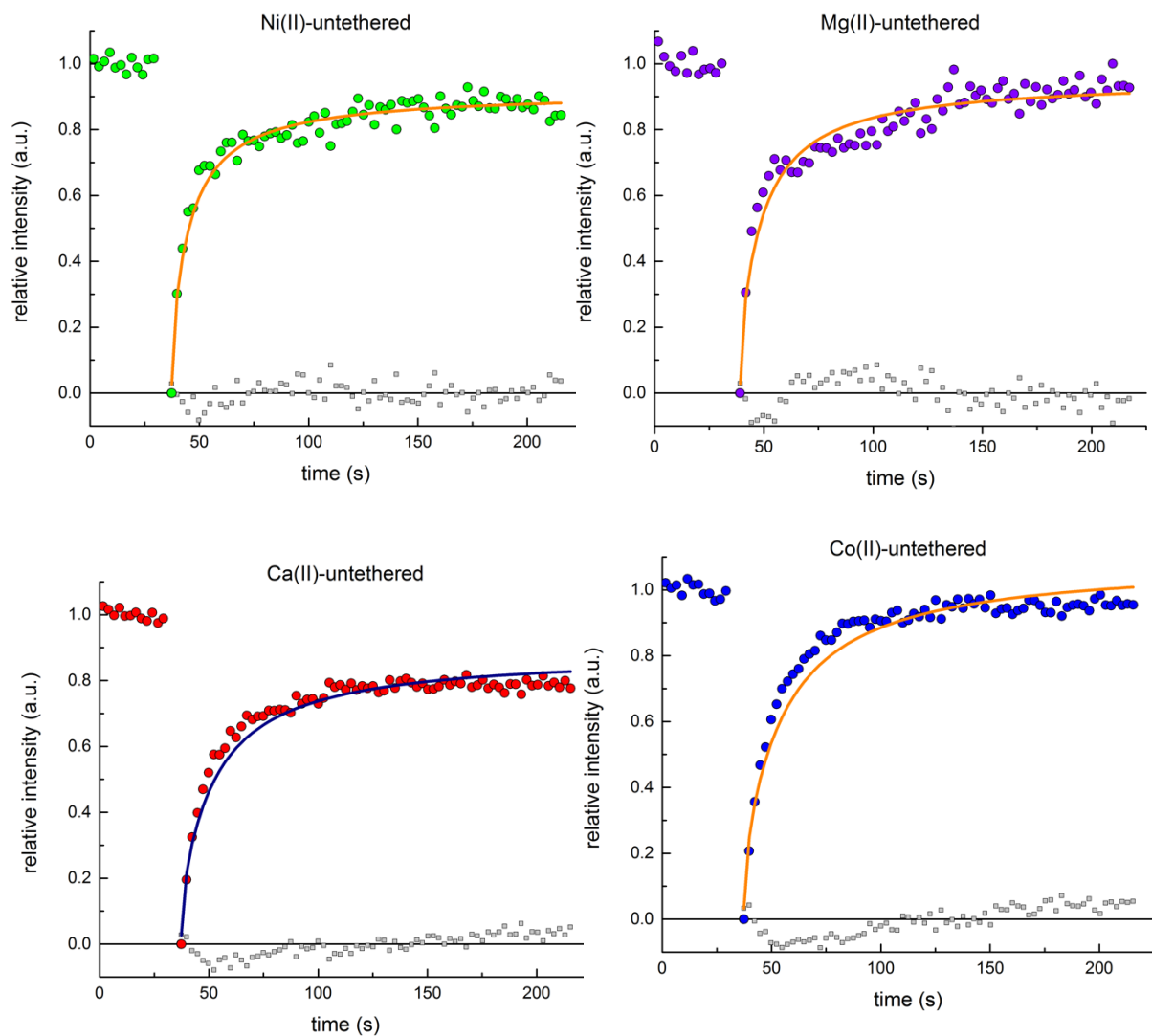


**Figure 3-4. Plot of time (s) vs. relative intensity. These data were obtained from a single FRAP experiment with perylene in an MP monolayer. Grey squares represent residuals for each recovery curve.**

The resulting fits of the normalized experimental data to Eq. 2 yield the  $D_T$  values shown in Table 3-2.  $D_T$  in the M(II)-bisphosphonate films are seen to depend on the identity of the metal ion, with the Co-bisphosphonate monolayer exhibiting significantly lower diffusion than the Ni-bisphosphonate and Mg-bisphosphonate monolayers. With the exception of the Co-bisphosphonate, the values of  $D_T$  in the M(II)-bisphosphonate films are a factor of two larger than those measured for In(III)-bisphosphonate films and a factor of 4 larger than is seen in Zr(IV)-bisphosphonate films.<sup>51</sup>

As discussed above,  $D_T$  is the fundamental physical quantity of interest, and it is instructive to relate  $D_T$  to the fluid properties of the monolayer. A useful gauge of fluid behavior is the viscosity of the medium,  $\eta$ , which is related to the translational diffusion constant and the size of the diffusing entity through the Stokes-Einstein equation (Eq. 4)

$$\frac{k_B T}{6 D_T r} \tag{4}$$

In Eq. 4  $k_B T$  is the thermal energy ( $T = 293$  K), and  $r$  is the radius of the diffusing molecule. The hydrodynamic volume of perylene is  $225 \text{ \AA}^3$ , yielding a value of  $r = 3.8 \text{ \AA}$ . The effective viscosities of the monolayers studied here are given in Table 3-2. For purposes of comparison, the viscosity of glycerol is *ca.* 1410 cP at room temperature.<sup>51</sup>

**Table 3-2. Average  $D_T$  values and calculated viscosities for MP monolayers with an untethered chromophore.**

Surface	$D_T$ ( $\mu\text{m}^2/\text{s}$ )	$\eta$ (cP)
Ni(II)- $\text{O}_3\text{P}-\text{C}_8\text{H}_{16}-\text{PO}_3\text{H}$	$3.33 \pm 0.97$	$170 \pm 50$
Mg(II)- $\text{O}_3\text{P}-\text{C}_8\text{H}_{16}-\text{PO}_3\text{H}$	$2.85 \pm 0.78$	$198 \pm 54$
Ca(II)- $\text{O}_3\text{P}-\text{C}_8\text{H}_{16}-\text{PO}_3\text{H}$	$2.00 \pm 0.45$	$282 \pm 63$
Co(II)- $\text{O}_3\text{P}-\text{C}_8\text{H}_{16}-\text{PO}_3\text{H}$	$1.30 \pm 0.56$	$434 \pm 187$
In(III)- $\text{O}_3\text{P}-\text{C}_8\text{H}_{16}-\text{PO}_3\text{H}$	$0.63 \pm 0.17$	$895 \pm 242$
Zr(IV)- $\text{O}_3\text{P}-\text{C}_8\text{H}_{16}-\text{PO}_3\text{H}$	$0.31 \pm 0.10$	$1810 \pm 584$

Surface	$D_T$ ( $\mu\text{m}^2/\text{s}$ )	$\eta$ (cP)
$\text{HO}_3\text{P}-\text{O}-\text{CO}_2-\text{C}_7\text{H}_{15}$	$0.18 \pm 0.02$	$3140 \pm 349$

The derived viscosities (Table 3-2) underscore that the monolayers behave as viscous liquids. This behavior can be ascribed to two different properties within the adlayer. The first is the intermolecular forces among the monolayer constituents, especially those in the aliphatic chain region, and the second is the extent of equilibrium exchange of monolayer constituents that is mediated by dissociation and association of the metal-phosphonate complex at the support surface. While the characterization of a free chromophore is sensitive to both of these molecular-scale interactions within the monolayer, it is possible to study complementary systems to resolve the relative importance of each contribution.

One limiting case is to eliminate the mobility of the monolayer constituents by bonding them covalently to the support surface (Figure 3-2). Ellipsometric data confirms the presence of

the monolayer ( $d = 17 \pm 1 \text{ \AA}$ ). FRAP measurements of perylene confined within the monolayer yielded  $D_T = 0.18 \pm 0.02 \text{ \mu m}^2/\text{s}$ , a value that is significantly lower than that seen for the MP monolayers. This finding suggests the importance of equilibrium exchange of monolayer constituents in determining the fluid properties of these monolayers.

*Tethered chromophore diffusion.* A perylene derivative capable of incorporation as a monolayer constituent, N,N'-bis(4-phosphonobutyl)-3,4,9,10-perylenediimide (BPDI) has been described previously and contains a terminal phosphonate functionality to allow participation in the formation of the bisphosphonate monolayer.<sup>72</sup> BPDI is a tethered chromophore, allowing evaluation of the exchange dynamics at the metal-phosphonate interface. The central question in the interpretation of FRAP data is whether the time-scale of equilibrium exchange of BPDI is short or long relative to the time-scale that is characteristic of the diffusion of a free species in the monolayer (Figure 3-5). If the chromophore exchange rate is slow relative to free chromophore diffusion, then the recovered value of  $D_T$  will be independent of the bleached spot size.<sup>16, 50</sup> FRAP data for each of the M(II)-bisphosphonate monolayers containing BPDI is shown in Figure 3-6. The recovery dynamics differ significantly from those of the untethered chromophore (Figure 3-4). Due to the functional form of the FRAP data, a model must be used that can account for a tethered chromophore, where diffusion and exchange both contribute.

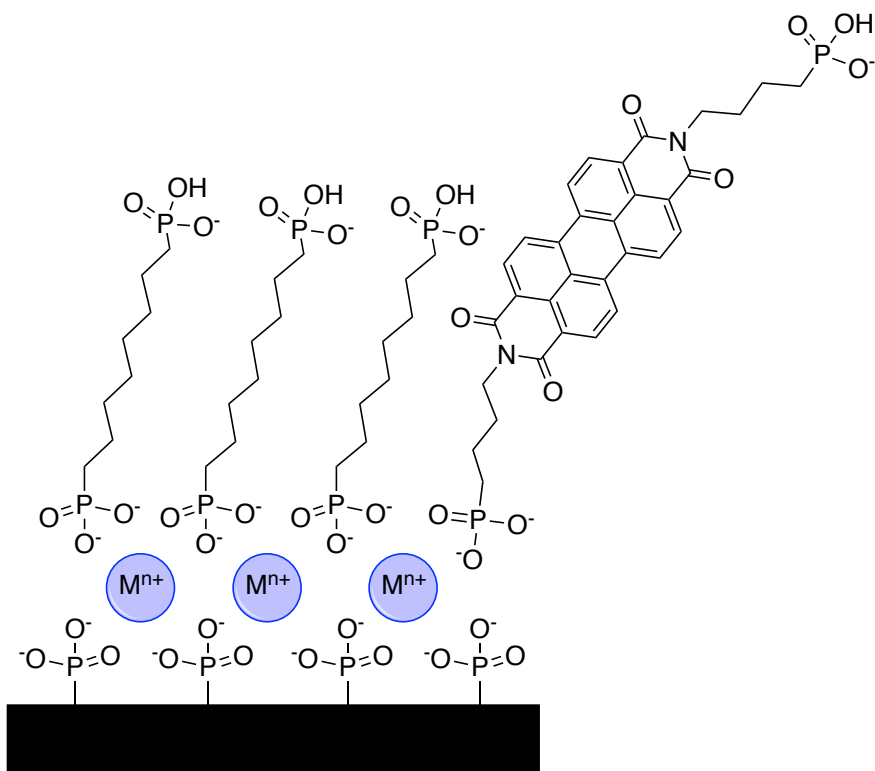


**Figure 3-5. BDPI incorporated in a MP monolayer. The protonation of the oxygens involved in metal binding depends on charge balance and for the sake of clarity are shown unprotonated here.**

The dynamics sensed with tethered chromophores are determined largely by the exchange equilibrium of the metal-phosphonate moiety. The relative rates of interfacial association and dissociation need to be considered in the extraction of  $D_T$  from the FRAP data. If the association and dissociation kinetics are fast relative to the time-scale of chromophore translational motion, the observed translational diffusion will resemble that seen for the free chromophore.<sup>16, 50</sup> We do not observe that similarity in our data. We model these data in the limit of association and dissociation kinetics being slow relative to translational motion. This matter can be evaluated by performing FRAP measurements for a range of photobleached spot

radii ( $\omega$ ). If the FRAP data are independent of spot size, association and dissociation kinetics are demonstrated to be slow, and we observe this limit experimentally (Table 3-3). The FRAP decay data shown in Figure 3-6 are consistent with contributions to the signal from both translational diffusion and association and dissociation from the interface.

**Table 3-3.  $D_T$  values for M(II)P monolayers with a tethered chromophore at varying bleach radii ( $\omega$ ) showing no dependence.**

Surface	$(D_T) \mu^2/s$ $\omega = 10\mu$	$(D_T) \mu^2/s$ $\omega = 15\mu$
Mg(II)- O <sub>3</sub> PC <sub>8</sub> H <sub>16</sub> PO <sub>3</sub> H	0.20 ± 0.10	0.26 ± 0.13
Co(II)- O <sub>3</sub> PC <sub>8</sub> H <sub>16</sub> PO <sub>3</sub> H	0.32 ± 0.26	0.57 ± 0.19
Ni(II)- O <sub>3</sub> PC <sub>8</sub> H <sub>16</sub> PO <sub>3</sub> H	0.34 ± 0.27	0.63 ± 0.47
Ca(II)- O <sub>3</sub> PC <sub>8</sub> H <sub>16</sub> PO <sub>3</sub> H	0.49 ± 0.40	0.57 ± 0.39

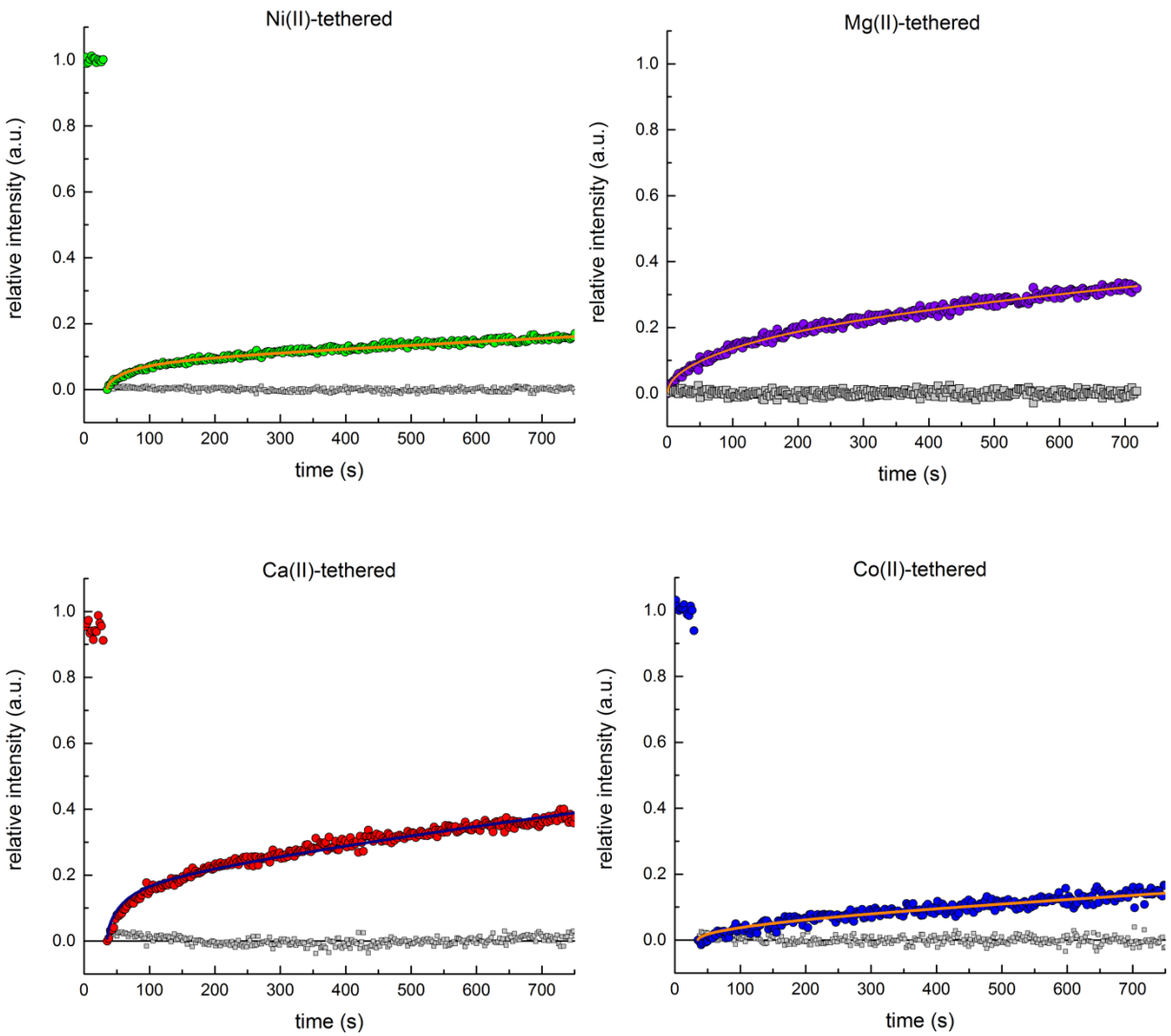


**Figure 3-6. Plot of time (s) vs. relative intensity. These data were obtained from a single FRAP experiment with BDPI in an MP monolayer. Grey squares represent residuals for each recovery curve.**

The FRAP decays must thus be modeled using the full reaction-diffusion model (Eq. 5).<sup>72</sup>

$$I_{norm}(t) = L^{-1} \left[ \frac{1}{p} \left( \frac{F_{eq}}{p} + 1 - 2K_1(q) \right) I_1(q) \right] + \frac{k_{on}^*}{p} + \frac{B_{eq}}{p} \frac{1}{k_{off}}$$

$$q = \frac{p}{D_T} + 1 + \frac{k_{on}^*}{p} \frac{1}{k_{off}} \quad (5)$$

$$k_{on}^* = k_{on}[m]$$

Where  $p$  is the Laplace variable that inverts to yield time,  $L^{-1}$  indicates the inverse Laplace transform of the function contained in brackets,  $\omega$  is the radius of the bleached spot, and the terms  $K_1$  and  $I_1$  are modified Bessel functions. The terms  $F_{eq}$  (equilibrium free concentration) and  $B_{eq}$  (equilibrium bound concentration) are related to  $k_{on}^*$  and  $k_{off}$  by fitting the data in Figure 6 to Eq. 5 yield values for  $k_{on}^*$  and  $k_{off}$  shown in Table 3-4.

$$\frac{F_{eq}}{B_{eq}} = 1 + \frac{k_{off}}{k_{on}^*} + \frac{B_{eq}}{k_{on}^*} \frac{1}{k_{off}} \quad (6)$$

**Table 3-4.  $D_T$  and  $k_{on}^*$  and  $k_{off}$  values for MP monolayers with a tethered chromophore.**

Surface	Diffusion constant ( $D_T$ ) $\mu\text{m}^2/\text{s}$	$k_{on}^*$	$k_{off}$	$K_{eq}^*$
Mg(II)- $\text{O}_3\text{P-C}_8\text{H}_{16}\text{-PO}_3\text{H}$	$0.20 \pm 0.10$	$(4.1 \pm 4.2) \times 10^{-4}$	$(8.3 \pm 3.7) \times 10^{-4}$	$0.49 \pm 0.51$
Co(II)- $\text{O}_3\text{P-C}_8\text{H}_{16}\text{-PO}_3\text{H}$	$0.32 \pm 0.26$	$(1.4 \pm 0.9) \times 10^{-4}$	$(8.6 \pm 7.7) \times 10^{-4}$	$0.16 \pm 0.10$
Ni(II)- $\text{O}_3\text{P-C}_8\text{H}_{16}\text{-PO}_3\text{H}$	$0.34 \pm 0.27$	$(2.4 \pm 1.6) \times 10^{-4}$	$(7.4 \pm 3.8) \times 10^{-4}$	$0.34 \pm 0.22$
Ca(II)- $\text{O}_3\text{P-C}_8\text{H}_{16}\text{-PO}_3\text{H}$	$0.49 \pm 0.40$	$(4.9 \pm 3.3) \times 10^{-4}$	$(8.9 \pm 6.8) \times 10^{-4}$	$0.55 \pm 0.37$
In(III)- $\text{O}_3\text{P-C}_8\text{H}_{16}\text{-PO}_3\text{H}$	$0.52 \pm 0.11$	$(6.8 \pm 1.4) \times 10^{-5}$	$(2.8 \pm 1.9) \times 10^{-4}$	$0.24 \pm 0.05$
Zr(IV)- $\text{O}_3\text{P-C}_8\text{H}_{16}\text{-PO}_3\text{H}$	$0.49 \pm 0.22$	$(1.3 \pm 0.4) \times 10^{-4}$	$(8.6 \pm 2.7) \times 10^{-4}$	$0.15 \pm 0.05$

The values of  $D_T$ ,  $k_{on}^*$  and  $k_{off}$  for BPDI in the M(II)-bisphosphonate monolayers are shown in Table 3-4 and are independent of divalent metal ion identity to within the experimental uncertainty, save for Ni(II). The implication of these findings is that the exchange dynamics of the metal-phosphonate interface are similar for all M(II)-bisphosphonate monolayers reported here. The  $D_T$  values for the tethered chromophore system can also be compared to those reported for the untethered chromophore (Table 3-2). The  $D_T$  values for the tethered chromophore system with the M(II)P films are 4 to 10 times smaller than those for the free chromophore. The difference between free and tethered chromophore  $D_T$  is less substantial for In(III)-bisphosphonate and Zr(IV)-bisphosphonate films, indicating that the equilibrium dynamics for these monolayers plays a more important role for determining the properties of these monolayers.

It is interesting to determine the effective  $K_{eq}$  for these systems from the quantities  $k_{on}^*$  and  $k_{off}$  (Table 3-4). We find that these  $K_{eq}$  values are the same to within the experimental uncertainty for the divalent metal ions an, with a slight metal ion-dependence. These data are interesting, but it is important to keep in mind that differences between metal ions will be masked by the contribution of diffusional processes.

### **3.5 Conclusion**

Our studies of chromophore diffusion in M(II)-bisphosphonate monolayers demonstrate that the metal ion does indeed play a role in the organization and, more importantly, the dynamics of this family of monolayers. Monolayers formed using divalent metals exhibit more facile chromophore translational diffusion than is seen for a free chromophore in In(III)-bisphosphonate and Zr(IV)-bisphosphonate monolayers. Differences in packing density and film organization account for the difference seen in the translational dynamics of these MP

monolayers. For studies using a tethered chromophore, the results are consistent with the equilibrium dynamics of the monolayer playing an important, metal ion dependent role in their fluid properties. The M(II)-bisphosphonate monolayers exhibited similar properties, which were different from those seen for In(III) and Zr(IV). All of the MP films we have considered function as viscous liquids, which may have implications for future applications of these systems.

## **REFERENCES**

## REFERENCES

1. Dubois, L. H., Self-Assembled Monolayers as Models for Organic-Surfaces. *Abstr Pap Am Chem S* **1992**, 204, 92-Phys.
2. Ulman, A., Formation and structure of self-assembled monolayers. *Chem Rev* **1996**, 96 (4), 1533-1554.
3. Love, J. C.; Estroff, L. A.; Kriebel, J. K.; Nuzzo, R. G.; Whitesides, G. M., Self-assembled monolayers of thiolates on metals as a form of nanotechnology. *Chem Rev* **2005**, 105 (4), 1103-1169.
4. Badia, A.; Lennox, R. B.; Reven, L., A dynamic view of self-assembled monolayers. *Accounts of Chemical Research* **2000**, 33 (7), 475-481.
5. Schreiber, F., Structure and growth of self-assembling monolayers. *Prog Surf Sci* **2000**, 65 (5-8), 151-256.
6. Sagiv, J.; Polymeropoulos, E. E., Adsorbed monolayers. Molecular organization and electrical properties. *Berichte der Bunsen-Gesellschaft* **1978**, 82 (9), 882.
7. Sagiv, J., Organized Monolayers by Adsorption .1. Formation and Structure of Oleophobic Mixed Monolayers on Solid-Surfaces. *J Am Chem Soc* **1980**, 102 (1), 92-98.
8. Sagiv, J., Organized monolayers by adsorption. II. Molecular orientation in mixed dye monolayers built on anisotropic polymeric surfaces. *Israel Journal of Chemistry* **1980**, 18 (3-4), 339-45.
9. Sagiv, J., Organized monolayers by adsorption. III. Irreversible adsorption and memory effects in skeletonized silane monolayers. *Israel Journal of Chemistry* **1980**, 18 (3-4), 346-53.
10. Netzer, L.; Sagiv, J., A new approach to construction of artificial monolayer assemblies. *J Am Chem Soc* **1983**, 105 (3), 674-6.
11. Netzer, L.; Iscovici, R.; Sagiv, J., Adsorbed monolayers versus Langmuir-Blodgett monolayers - why and how? I. From monolayer to multilayer, by adsorption. *Thin Solid Films* **1983**, 99 (1-3), 235-41.
12. Netzer, L.; Iscovici, R.; Sagiv, J., Adsorbed monolayers versus Langmuir-Blodgett monolayers - why and how? II. Characterization of built-up films constructed by stepwise adsorption of individual monolayers. *Thin Solid Films* **1983**, 100 (1), 67-76.
13. Byrd, H.; Snover, J. L.; Thompson, M. E., Mechanistic Studies of Film Growth of Zirconium Bis(Phosphonate) Monolayer and Multilayer Thin-Films - These Things Grow Darned Flat. *Langmuir* **1995**, 11 (11), 4449-4453.

14. Lee, H.; Kepley, L. J.; Hong, H. G.; Akhter, S.; Mallouk, T. E., Adsorption of Ordered Zirconium Phosphonate Multilayer Films on Silicon and Gold Surfaces. *J Phys Chem-US* **1988**, *92* (9), 2597-2601.
15. Snover, J. L.; Byrd, H.; Suponeva, E. P.; Vicenzi, E.; Thompson, M. E., Growth and characterization of photoactive and electroactive zirconium bisphosphonate multilayer films. *Chemistry of Materials* **1996**, *8* (7), 1490-1499.
16. Cinier, M.; Petit, M.; Williams, M. N.; Fabre, R. M.; Pecorari, F.; Talham, D. R.; Bujoli, B.; Tellier, C., Bisphosphonate Adaptors for Specific Protein Binding on Zirconium Phosphonate-based Microarrays. *Bioconjugate Chem* **2009**, *20* (12), 2270-2277.
17. Cao, G.; Hong, H. G.; Mallouk, T. E., Layered Metal Phosphates and Phosphonates - from Crystals to Monolayers. *Accounts of Chemical Research* **1992**, *25* (9), 420-427.
18. Katz, H. E., Multilayer Deposition of Novel Organophosphonates with Zirconium(IV). *Chemistry of Materials* **1994**, *6* (12), 2227-2232.
19. Ansell, M. A.; Cogan, E. B.; Neff, G. A.; von Roeschlaub, R.; Page, C. J., Self-assembly of thin film superstructures based on alternating metal-bisphosphonate and cobalt diisocyanide layers. *Supramol. Sci.* **1997**, *4* (1-2), 21-26.
20. Ansell, M. A.; Zeppenfeld, A. C.; Yoshimoto, K.; Cogan, E. B.; Page, C. J., Self-assembled cobalt-diisocyanobenzene multilayer thin films. *Chemistry of Materials* **1996**, *8* (3), 591-&.
21. Neff, G. A.; Page, C. J.; Meintjes, E.; Tsuda, T.; Pilgrim, W. C.; Roberts, N.; Warren, W. W., Hydrolysis of surface-bound phosphonate esters for the self-assembly of multilayer films: Use of solid state magic angle spinning P-31 NMR as a probe of reactions on surfaces. *Langmuir* **1996**, *12* (2), 238-242.
22. O'Brien, J. T.; Zeppenfeld, A. C.; Richmond, G. L.; Page, C. J., Fourier-Transform Infrared-Spectroscopy Studies of Hafnium Alkylbis(Phosphonate) Multilayers On Gold - Effects of Alkylbis(Phosphonate) Chain-Length, Substrate Roughness, and Surface Functionalization On Film Structure and Order. *Langmuir* **1994**, *10* (12), 4657-4663.
23. Zeppenfeld, A. C.; Fiddler, S. L.; Ham, W. K.; Klopfenstein, B. J.; Page, C. J., Variation of Layer Spacing in Self-Assembled Hafnium-1,10-Decanediybis(Phosphonate) Multilayers As Determined By Ellipsometry and Grazing Angle X-Ray-Diffraction. *J Am Chem Soc* **1994**, *116* (20), 9158-9165.
24. Kohli, P.; Rini, M. C.; Major, J. S.; Blanchard, G. J., Elucidating the balance between metal ion complexation and polymer conformation in maleimide vinyl ether polymer multilayer structures. *Journal of Materials Chemistry* **2001**, *11* (12), 2996-3001.
25. Yang, H. C.; Aoki, K.; Hong, H. G.; Sackett, D. D.; Arendt, M. F.; Yau, S. L.; Bell, C. M.; Mallouk, T. E., Growth and Characterization of Metal(II) Alkanebisphosphonate Multilayer Thin-Films on Gold Surfaces. *J Am Chem Soc* **1993**, *115* (25), 11855-11862.

26. Baumler, S. M.; Reidy, T. M.; Blanchard, G. J., Diffusional motion as a gauge of fluidity and interfacial adhesion. Supported alkylphosphonate monolayers. *Journal of Colloid and Interface Science* **2016**, *468*, 145-155.
27. Livingston, C.; Blanchard, G. J., Metal Ion-Dependent Interfacial Organization and Dynamics of Metal-Phosphonate Monolayers. *Langmuir* **2021**, *37* (15), 4658-4665.
28. Horne, J. C.; Blanchard, G. J., Dynamics within a single molecular layer. Aggregation, relaxation, and the absence of motion. *Journal of the American Chemical Society* **1996**, *118* (50), 12788-12795.
29. Shannon, R. D., Revised Effective Ionic-Radii and Systematic Studies of Interatomic Distances in Halides and Chalcogenides. *Acta Crystallogr A* **1976**, *32* (Sep1), 751-767.
30. Cao, G.; Lynch, V. M.; Swinnea, J. S.; Mallouk, T. E., Synthesis and Structural Characterization of Layered Calcium and Lanthanide Phosphonate Salts. *Inorg Chem* **1990**, *29* (11), 2112-2117.
31. Cao, G.; Lee, H.; Lynch, V. M.; Mallouk, T. E., Synthesis and structural characterization of a homologous series of divalent-metal phosphonates,  $MII(O_3PR).n \cdot H_2O$  and  $MII(HO_3PR)_2$ . *Inorganic Chemistry* **1988**, *27* (16), 2781-2785.
32. Cristiano, P.; Vieira, S. F.; Longhini, A. L.; Lydic, T.; Asare-Bediako, B.; Hammer, S. S.; Hossain, M.; Crossman, D.; Sielski, M. S.; Adu-Agyeiwaah, Y.; Dupont, M.; Floyd, J. L.; Li Calzi, S.; Blanchard, G. J.; Busik, J. V.; Grant, M. B., Selective LXR agonist, DMHCA, corrects the Retina-bone Marrow Axis in Type 2 Diabetes. *J. Clin. Invest.* **2020**, *5* (137320), 1-21.
33. Soumpasis, D. M., Theoretical-Analysis of Fluorescence Photobleaching Recovery Experiments. *Biophys J* **1983**, *41* (1), 95-97.
34. Segur, J. B.; Oberstar, H. E., Viscosity of Glycerol and Its Aqueous Solutions. *Ind Eng Chem* **1951**, *43* (9), 2117-2120.
35. Sprague, B. L.; Pego, R. L.; Stavreva, D. A.; McNally, J. G., Analysis of binding reactions by fluorescence recovery after photobleaching. *Biophys J* **2004**, *86* (6), 3473-3495.

## **Chapter Four: Effect of Monolayer Constituent Structural Modification on the Constituent Diffusional Properties of Metal Phosphonate Monolayers**

## 4.1 Abstract

Self-assembled monolayers (SAMs) are a surface modification of broad interest and application due to their ease of synthesis and structural variability. In particular, metal-bisphosphonate films are easy to modify for specific applications and can be synthesized in aqueous media at room temperature. The  $\omega$ -terminal group identity of the metal-phosphonate monolayer was varied to determine its effect on monolayer dynamics.

## 4.2 Introduction

The importance of self-assembled monolayers (SAMs) and the use of metal-phosphonate (MP) films in surface modification have been well established previously in this dissertation. Metal-phosphonate films that have been described here have featured a phosphate terminated surface, that is then bound to a metal, followed by a C<sub>8</sub>  $\alpha,\omega$ -alkanebisphosphonate (Figure 4-1). While this is one of the most common structural motifs for MP films, the terminal group has often been modified and the effect of such modification on monolayer constituent dynamics remains to be determined.

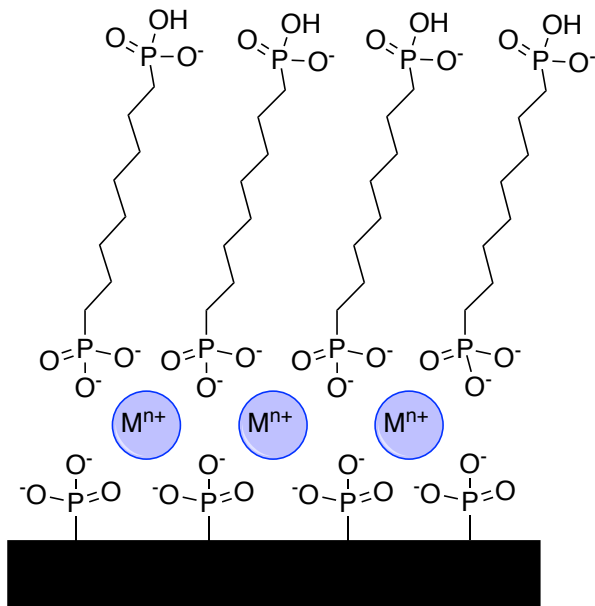


**Figure. 4-1. Schematic of metal-phosphonate monolayer. The protonation of the oxygens involved in metal binding depends on charge balance and for the sake of clarity are shown unprotonated here.**

Many different bisphosphonates have been used in MP films. An increase from an 8-carbon aliphatic chain to a 12-carbon aliphatic chain has been reported previously.<sup>8</sup> Many bisphosphonates that incorporate aromatic chromophores have been used for their optical properties.<sup>7, 34, 61, 63</sup> Bisphosphonates that mimic biological compounds for use in protein and DNA binding have been synthesized for use in MP films.<sup>3, 62</sup> While the structural integrity of these MP films has been investigated extensively, the translational diffusion properties of the monolayer constituents in these films has received substantially less attention. It is this property, however, that is relevant to the function of these monolayers as bound fluid films.

The Blanchard group has reported previously on the rotational dynamics of monolayer constituents in zirconium-bisphosphonate (ZP) monolayers.<sup>7, 8</sup> Oligothiophene chromophores of varying lengths, corresponding to the length of the analogous bisphosphonate, were used (Figure 4-2). Limited rotation within the monolayers for both films was observed.<sup>7, 8</sup>

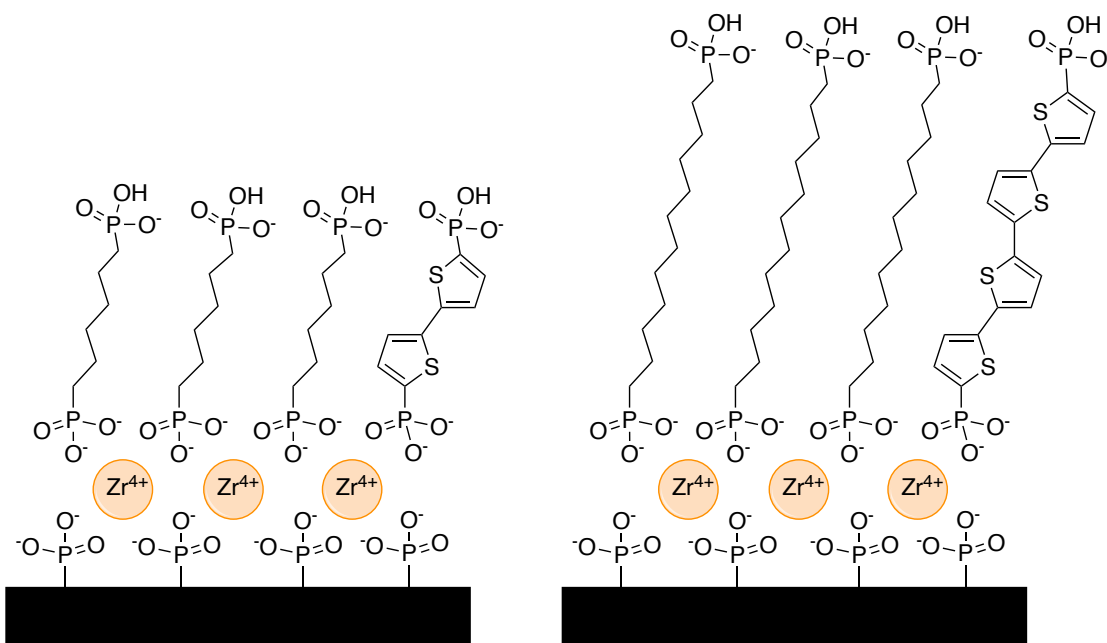


**Figure 4-2. Scheme of ZP films with oligothiophene chromophores**

The emphasis of the work in this dissertation thus far has been on the effect of metal ion charge and identity on translational diffusion and layer organization. In addition to the metal-phosphonate interactions, the structure and terminal group identity of the monolayer constituents can play a role in the observed dynamics and we provide data on the influence(s) of capping the monolayer with a metal ion, changing the length of the monolayer aliphatic chain, and removing the  $\omega$ -terminal phosphonate functionality.

### 4.3 Experimental

*Chemicals used:* Concentrated sulfuric acid, 2,4,6-collidine,  $\text{In}(\text{NO}_3)_3 \cdot x\text{H}_2\text{O}$ , octanoyl chloride,  $\text{POCl}_3$ , perylene, octylphosphonic acid, 1,8-octanebisphosphonic acid, and 1,12-dodecanebisphosphonic acid were obtained from Sigma-Aldrich in their highest purity forms and used without further purification. Dodecylphosphonic acid was obtained from Alfa Aesar (95%) and used without further purification.  $\text{MgCl}_2 \cdot 6\text{H}_2\text{O}$  (99%) was obtained from CCI Chemical and used without further purification. All water was purified using a Milli-Q purification system.

*Metal bisphosphonate monolayer synthesis.* Piranha solution (*Caution! Strong oxidizer!*) was used to clean glass or oxidized silicon plates (1cm x 1cm) that were used as monolayer supports. Plates were immersed in piranha solution for 15 minutes. The plates were then rinsed with 18 M $\Omega$  water and immersed in a 2M HCl solution for 5 minutes. The plates were rinsed with 18 M $\Omega$  water and then with anhydrous acetonitrile. The surface was immediately phosphorylated by immersion in 100 mM  $\text{POCl}_3$  and 100 mM 2,4,6-collidine in dry acetonitrile for one hour, then rinsed with anhydrous acetonitrile. The plates were then treated overnight with 5 mM metal ion solution,  $\text{MgCl}_2 \cdot 6\text{H}_2\text{O}$ ,  $\text{ZrOCl}_2$ , or  $\text{In}(\text{NO}_3)_3 \cdot x \text{H}_2\text{O}$ .<sup>73,7</sup> For reasons of solubility, 100% ethanol was used as the solvent for solutions containing  $\text{MgCl}_2 \cdot 6\text{H}_2\text{O}$  and a 60% EtOH/ 40%  $\text{H}_2\text{O}$  solvent mixture was used for Zr(IV) and In(III).<sup>27</sup> After washing with Milli-Q water, the plates were treated with 1.25 mM octylphosphonic acid or 1,8-octanebisphosphonic acid in ethanol for one hour. 1,12-dodecanebisphosphonic acid was also used, but due to solubility reasons, has to be in water, therefore these films were only made with  $\text{Zr}^{4+}$  and  $\text{In}^{3+}$ . The pH of all metal ion-containing and phosphonate-containing solutions was maintained between 2 and 4 using dilute HCl to minimize the formation of metal hydroxides.

For substrates used to perform FRAP measurements, the phosphonate solution contained 1 mol% of perylene.

*Fluorescence Recovery After Photobleaching (FRAP).* A Nikon C2+ confocal laser scanning microscopy system with a Nikon Eclipse Ti-E inverted microscope with a confocal scanning system (Nikon Ti-S-CON) was utilized for acquiring FRAP data. A 20× objective lens was used for all experiments. The chromophore (perylene) was excited at 405 nm with a diode laser (Nikon Lu-N4) and detected using a PMT detector system (Nikon C2-DU3, 400nm-700nm). The initial intensity was measured for 30 sec, bleached for 5 sec, and recovery was monitored for a minimum of 3 minutes. A minimum of ten spots across each monolayer were measured.

#### 4.4 Results and Discussion

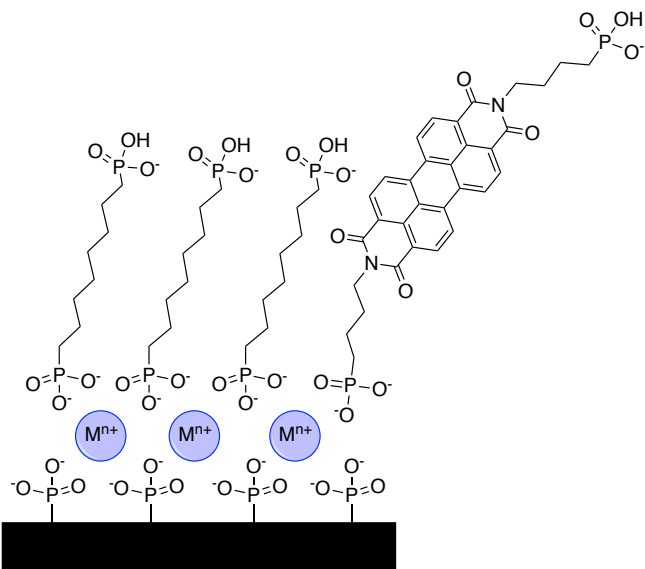


**Figure 4-3. BDPI incorporated in a MP monolayer. The protonation of the oxygens involved in metal binding depends on charge balance and for the sake of clarity are shown unprotonated here.**

With the role of the metal-bisphosphonate equilibrium dynamics evaluated and reported in previous chapters. Briefly, the metal-phosphonate interactions were investigated by FRAP using a tethered chromophore (Figure 4-3). It has been shown that the metal-phosphonate association and dissociation kinetics are not dependent on metal ion charge or identity (Table 4-1).<sup>70</sup> Metal ion charge did affect the organization and translational mobility of chromophores embedded in but not tethered to the monolayer, as seen through FRAP studies using perylene (Figure 4-4), where the fluidity of the film increases as charge decreases (Table 4-2).

**Table 4-1.  $D_T$  values for MP monolayers with a tethered chromophore.**

Surface	Diffusion constant ( $D_T$ ) $\mu\text{m}^2/\text{s}$
Mg(II)- O <sub>3</sub> P-C <sub>8</sub> H <sub>16</sub> -PO <sub>3</sub> H	0.20 ± 0.10
Co(II)- O <sub>3</sub> P-C <sub>8</sub> H <sub>16</sub> -PO <sub>3</sub> H	0.32 ± 0.26
Ni(II)- O <sub>3</sub> P-C <sub>8</sub> H <sub>16</sub> -PO <sub>3</sub> H	0.34 ± 0.27
Ca(II)- O <sub>3</sub> P-C <sub>8</sub> H <sub>16</sub> -PO <sub>3</sub> H	0.49 ± 0.40
In(III)- O <sub>3</sub> P-C <sub>8</sub> H <sub>16</sub> -PO <sub>3</sub> H	0.52 ± 0.11
Zr(IV)- O <sub>3</sub> P-C <sub>8</sub> H <sub>16</sub> -PO <sub>3</sub> H	0.49 ± 0.22

**Table 4-2. Average  $D_T$  values and calculated viscosities for MP monolayers with an untethered chromophore.**

Surface	$D_T$ ( $\mu\text{m}^2/\text{s}$ )	$\eta$ (cP)
Mg(II)- $\text{O}_3\text{P}-\text{C}_8\text{H}_{16}-\text{PO}_3\text{H}$	$3.33 \pm 0.97$	$170 \pm 50$
Co(II)- $\text{O}_3\text{P}-\text{C}_8\text{H}_{16}-\text{PO}_3\text{H}$	$2.85 \pm 0.78$	$198 \pm 54$
Ni(II)- $\text{O}_3\text{P}-\text{C}_8\text{H}_{16}-\text{PO}_3\text{H}$	$2.00 \pm 0.45$	$282 \pm 63$
Ca(II)- $\text{O}_3\text{P}-\text{C}_8\text{H}_{16}-\text{PO}_3\text{H}$	$1.30 \pm 0.56$	$434 \pm 187$
In(III)- $\text{O}_3\text{P}-\text{C}_8\text{H}_{16}-\text{PO}_3\text{H}$	$0.63 \pm 0.17$	$895 \pm 242$
Zr(IV)- $\text{O}_3\text{P}-\text{C}_8\text{H}_{17}$	$0.31 \pm 0.10$	$1810 \pm 584$

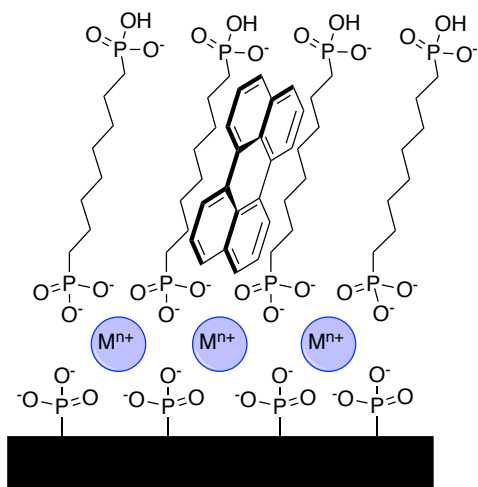


**Figure 4-4. Perylene incorporated in a MP monolayer. . The protonation of the oxygens involved in metal binding depends on charge balance and for the sake of clarity are shown unprotonated here.**

We are interested in understanding the role that the aliphatic chain region of the monolayers plays in mediating translational diffusion. Zr(IV), In(III), and Mg(II) were used in

forming the metal bisphosphonate linkage in these studies. These metal ions were chosen because they allow a comparison of metal ion charge, which is expected to play a role in the MP gallery organization. Many of the MP films that have been reported are formed using  $\alpha,\omega$ -bisphosphonates because of the ability of these monolayer constituents to form multilayer structures.<sup>6, 10, 11, 23, 24, 27, 63, 69, 74-79</sup> To evaluate the role of aliphatic region constituent structure, three different structural configurations were evaluated using monolayers formed with  $\alpha,\omega$ -bisphosphonates. These are (1) with the  $\omega$ -terminal phosphonate layer capped with the same metal ion used for complexation of the  $\alpha$ -phosphonate to the support, (2) the same monolayer with no metal ion capping (i.e.  $\omega$ -terminal phosphonate) and (3) the comparison of  $\omega$ -terminal phosphonate monolayers with C<sub>8</sub> and C<sub>12</sub> aliphatic chains. (Figure 4-5)

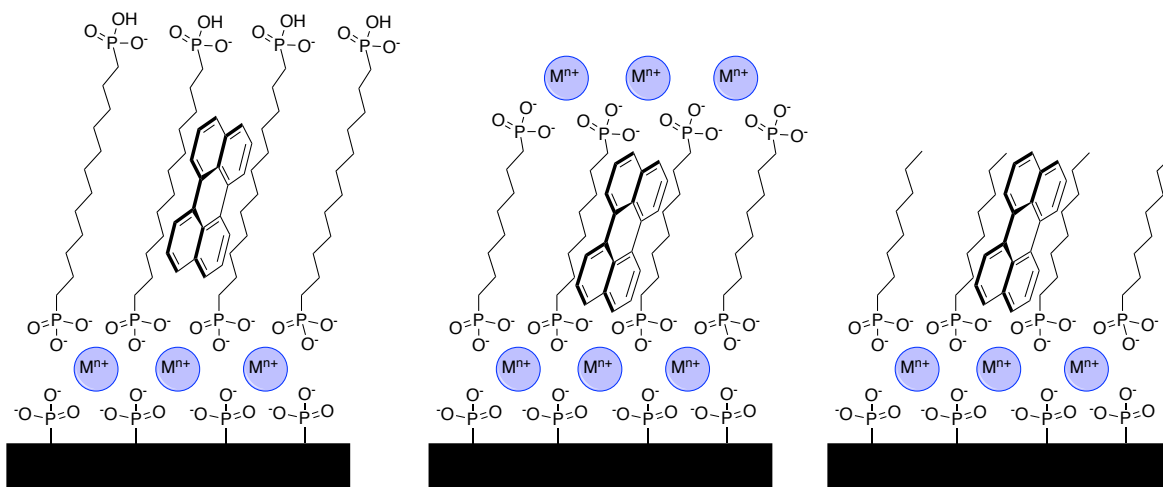


**Figure 4-5. Tail-end modification of MP monolayers including extending the aliphatic chain length, metal capping, and removing the terminal phosphonate.**

*Free chromophore diffusion.* The focus of these studies is on the aliphatic chain region, so we have used perylene as a free chromophore in the diffusion measurements used to characterize these monolayers. Perylene is not chemically bound to the monolayer which allows for free diffusion. When the chromophore is exposed to intense radiation during FRAP experiments, rapid photobleaching of the area of focus occurs, while slow photobleaching of the entire sample by the low intensity radiation is observable. Both of these phenomena are responsible for the overall FRAP signal, therefore the raw time-dependent intensity is normalized according to Eq. 1. The actual FRAP measurement consist of two selected regions of the same diameter, one acting as the reference and one that is photobleached.

$$I_{norm}(t) = \frac{I_{FRAP}(t) - I_{ref}(t) - I_{bleach}^{min}}{I_{pre-FRAP} - I_{pre-ref} - I_{bleach}^{min}} \quad (1)$$

The quantities in Eq. 1 are defined as follows.  $I_{norm}(t)$  is the normalized fluorescence recovery after photobleaching signal,  $I_{FRAP}(t)$  and  $I_{ref}(t)$  are the time-dependent fluorescence intensities acquired for the photobleached and reference regions, respectively,  $I_{bleach}^{min}$  is the lowest signal intensity in the FRAP measurement,  $I_{bleach}^{min} = I_{FRAP}(0) - I_{ref}(0)$ , and the intensities  $I_{pre-FRAP}$  and  $I_{pre-ref}$  are the fluorescence intensities in the selected regions prior to the photobleaching event. The functional form of the normalized recovery signal is given by Eq. 2 and is determined by the intermolecular interactions that mediate chromophore diffusion within the monolayer. In Eq. 2,  $I_0$  and  $I_1$  are modified Bessel functions of the first kind.<sup>16</sup>

$$I_{norm}(t) = \exp\left(-\frac{2\sqrt{D} \sqrt{t}}{w}\right) \left[ I_0\left(\frac{2\sqrt{D} \sqrt{t}}{w}\right) - I_1\left(\frac{2\sqrt{D} \sqrt{t}}{w}\right) \right] \quad (2)$$

We are interested in the translational diffusion constant  $D_T$  which is related to the radius of the photobleached region ( $w$ ) through the  $\tau_D$  term (Eq. 3).<sup>16</sup>  $\tau_D$  is extracted from fitting the experimental data to Eq. 2.<sup>50</sup>

$$D = \frac{2}{D_T} \quad (3)$$

The resulting fits of the normalized experimental data to Eq. 2 yield the  $D_T$  value. As discussed above,  $D_T$  is the fundamental physical quantity of interest, and it is instructive to relate  $D_T$  to the fluid properties of the monolayer. A useful gauge of fluid behavior is the viscosity of the medium,  $\eta$ , which is related to the translational diffusion constant and the size of the diffusing entity through the Stokes-Einstein equation (Eq. 4)

$$\frac{k_B T}{6 D_T r} \quad (4)$$

In Eq. 4  $k_B T$  is the thermal energy ( $T = 293$  K), and  $r$  is the radius of the diffusing molecule. The hydrodynamic volume of perylene is  $225 \text{ \AA}^3$ , yielding a value of  $r = 3.8 \text{ \AA}$ .

For the monolayers formed with 1,8-octanebisphosphonate and capped with metal ions, (Figure 4-5) we found that the presence of the metal ion at the monolayer top surface did not alter the value of  $D_T$  recovered for perylene for the Mg-bisphosphonate monolayer relative to that seen for the aliphatic-terminated monolayer (Table 4-3 and Figure 4-6). For the InP and ZP monolayers,  $D_T$  was seen to be slightly smaller than the values recovered for the aliphatic-terminated monolayers. This is an expected result because of the somewhat greater order enforced in the monolayer by the metal ion coordination at both the top and bottom monolayer surfaces.

**Table 4-3. Average  $D_T$  values and calculated viscosities for MP monolayers that have been capped with a metal with an untethered chromophore. For purposes of comparison, the viscosity of glycerol is *ca.* 1410 cP at room temperature.<sup>51</sup>**

Surface	$D_T$ ( $\mu\text{m}^2/\text{s}$ )	$\eta$ (cP)
Mg(II)- $\text{O}_3\text{P}-\text{C}_8\text{H}_{16}\text{PO}_3-\text{Mg}(\text{II})$	$2.51 \pm 1.20$	$225 \pm 108$
In(III)- $\text{O}_3\text{P}-\text{C}_8\text{H}_{16}\text{PO}_3-\text{In}(\text{III})$	$0.36 \pm 0.12$	$1570 \pm 523$
Zr(IV)- $\text{O}_3\text{P}-\text{C}_8\text{H}_{16}\text{PO}_3-\text{Zr}(\text{IV})$	$0.20 \pm 0.03$	$2820 \pm 423$

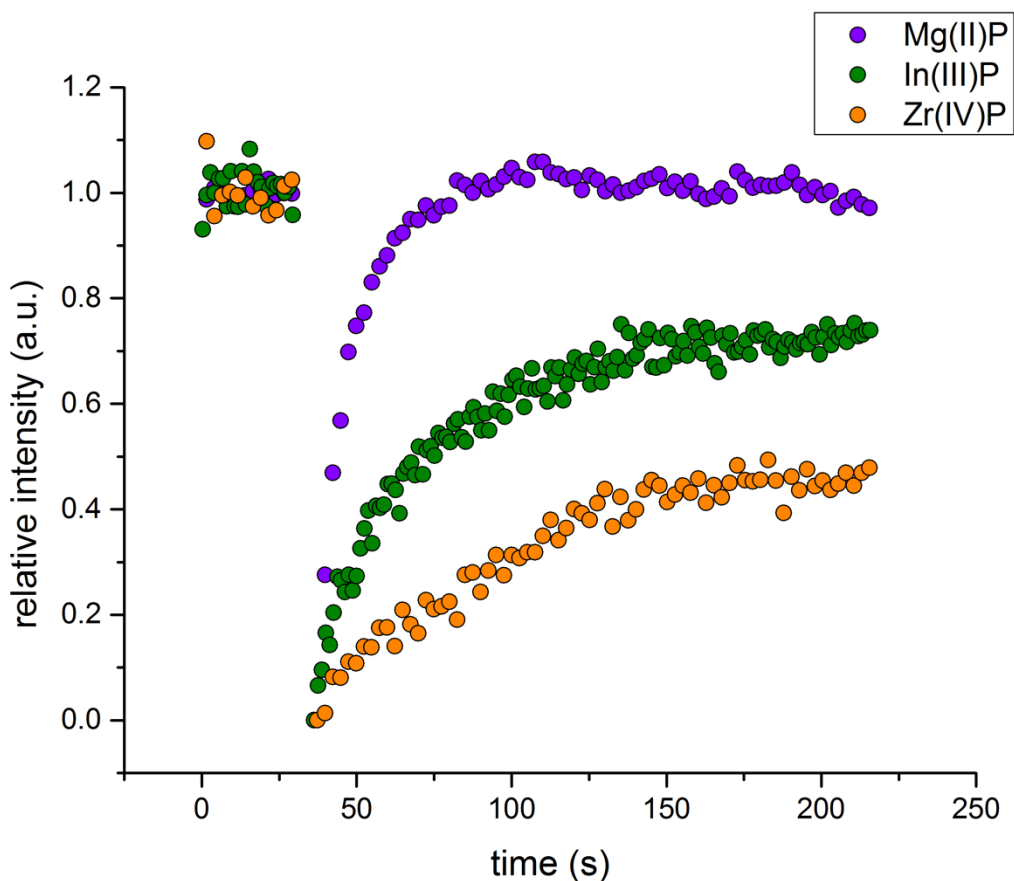


**Figure 4-6. Plot of time (s) vs. relative intensity of metal capped MP monolayers. These data were obtained from a FRAP measurement using perylene as the untethered chromophore.**

The values for  $D_T$  and  $\eta$  recovered for monolayers that possess an  $\omega$ -terminal phosphonate functionality but no metal ion cap exhibit slightly smaller  $D_T$  values for the Mg(II)-bisphosphonate and In(III)-bisphosphonate films compared to those seen for the metal ion-capped systems (Table 4-4 and Figure 4-7). The absence of the metal ion capping layer suggests that allowing the  $\omega$ -terminal phosphonates to interact directly with water and thus have their organization influenced primarily by H-bonding and dipolar interactions, gives rise to the ability of the aliphatic chains to play a somewhat more significant role in determining monolayer organization over the length scale sensed by the chromophore translational motion. Such a finding is consistent with the monolayer constituent spacing in MP monolayers being greater than the energetic optimum for aliphatic interchain interactions and being mediated by the spacing of the support surface phosphonate groups. The ZP monolayer exhibits the lowest perylene  $D_T$ , suggesting relatively tighter interchain spacing than is seen for the divalent metal ions.

**Table 4-4. Average  $D_T$  values and calculated viscosities for MP monolayers with the terminal phosphonate removed with an untethered chromophore. For purposes of comparison, the viscosity of glycerol is *ca.* 1410 cP at room temperature.<sup>51</sup>**

Surface	$D_T$ ( $\mu\text{m}^2/\text{s}$ )	$\eta$ (cP)
Mg(II)- O <sub>3</sub> P-C <sub>8</sub> H <sub>16</sub> -PO <sub>3</sub> H	0.84 ± 0.38	668 ± 302
In(III)- O <sub>3</sub> P-C <sub>8</sub> H <sub>16</sub> -PO <sub>3</sub> H	0.20 ± 0.02	2820 ± 282
Zr(IV)- O <sub>3</sub> P-C <sub>8</sub> H <sub>16</sub> -PO <sub>3</sub> H	0.24 ± 0.06	2350 ± 588

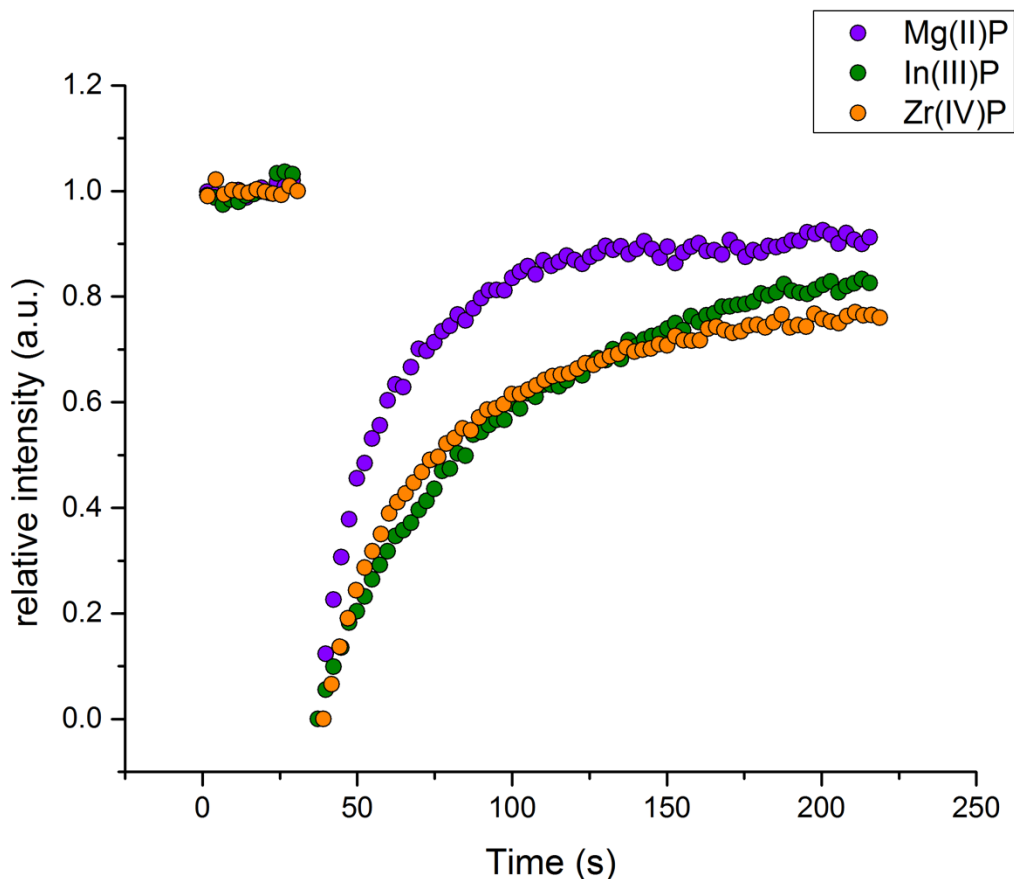


**Figure 4-7. Plot of time (s) vs. relative intensity of MP monolayers with the terminal phosphate removed. These data was obtained from a single FRAP experiment with perylene.**

Using the same  $\omega$ -phosphonate-terminated structural motif with a monolayer aliphatic chain length of 12 carbons rather than 8 carbons yields the perylene  $D_T$  and viscosity values shown in Table 4-5. Due to solubility properties, the 12 carbon M(II)-bisphosphonate films had to be synthesized in aqueous solutions, which does not allow for the formation of  $C_8$  M(II)-bisphosphonate monolayers. Therefore, only In(III)- and Zr(IV)- $C_{12}$  bisphosphonate monolayers were studied. Increasing the aliphatic chain length by four carbons does not have a measurable effect on  $D_T$  for the In(III)-bisphosphonate and Zr(IV)-bisphosphonate monolayers. While it is

possible that increasing the chain length could increase the mobility of the free chromophore due to the opportunity for increased interchain interactions, we did not observe any differences outside of the experimental uncertainty. These findings, taken collectively, indicate that the organization of MP monolayers is determined to the greatest extent by the organization of the support surface phosphonate groups, and that for the different metal ions studied, the monolayers are relatively similar, underscoring the importance of counter ions in controlling charge neutrality in the support-monolayer-metal ion layer.

**Table 4-5. Average  $D_T$  values and calculated viscosities for MP monolayers with a 12-carbon aliphatic chain with an untethered chromophore. For purposes of comparison, the viscosity of glycerol is *ca.* 1410 cP at room temperature.<sup>51</sup>**

Surface	$D_T$ ( $\mu\text{m}^2/\text{s}$ )	$\eta$ (cP)
In(III)-O <sub>3</sub> P-C <sub>12</sub> H <sub>24</sub> -PO <sub>3</sub> H	0.61 ± 0.35	925 ± 531
Zr(IV)-O <sub>3</sub> P-C <sub>12</sub> H <sub>24</sub> -PO <sub>3</sub> H	0.28 ± 0.12	2020 ± 866

#### 4.5 Conclusion

The role of the monolayer terminal functionality and aliphatic chain length are seen to be limited in determining diffusional properties. Metal ion capping of MP monolayers provided some evidence for slightly enhanced monolayer organization and the absence of  $\omega$ -terminal phosphonate functionality decreases the diffusion of the free chromophore, consistent with the MP monolayer organization being determined primarily by the support surface phosphonate density. All of the MP films we have considered in this work behave as viscous liquids, which is likely to have implications for future applications of these systems.

## REFERENCES

## REFERENCES

1. Horne, J. C.; Blanchard, G. J., The role of substrate identity in determining monolayer motional relaxation dynamics. *J Am Chem Soc* **1998**, *120* (25), 6336-6344.
2. Katz, H. E., Multilayer Deposition of Novel Organophosphonates with Zirconium(IV). *Chemistry of Materials* **1994**, *6* (12), 2227-2232.
3. Marcon, R. O.; Brochsztain, S., Characterization of self-assembled thin films of zirconium phosphonate/aromatic diimides. *Thin Solid Films* **2005**, *492* (1-2), 30-34.
4. Horne, J. C.; Blanchard, G. J., Dynamics within a single molecular layer. Aggregation, relaxation, and the absence of motion. *J Am Chem Soc* **1996**, *118* (50), 12788-12795.
5. Snover, J. L.; Byrd, H.; Suponeva, E. P.; Vicenzi, E.; Thompson, M. E., Growth and characterization of photoactive and electroactive zirconium bisphosphonate multilayer films. *Chemistry of Materials* **1996**, *8* (7), 1490-1499.
6. Cinier, M.; Petit, M.; Williams, M. N.; Fabre, R. M.; Pecorari, F.; Talham, D. R.; Bujoli, B.; Tellier, C., Bisphosphonate Adaptors for Specific Protein Binding on Zirconium Phosphonate-based Microarrays. *Bioconjugate Chem* **2009**, *20* (12), 2270-2277.
7. Lane, S. M.; Monot, J.; Petit, M.; Bujoli, B.; Talham, D. R., XPS investigation of DNA binding to zirconium-phosphonate surfaces. *Colloid Surface B* **2007**, *58* (1), 34-38.
8. Livingston, C.; Blanchard, G. J., Metal Ion Dependent Interfacial Organization and Dynamics of Metal Phosphonate Monolayers. *Langmuir* **2021**, *37*, xxx-xxx.
9. Yang, H. C.; Aoki, K.; Hong, H. G.; Sackett, D. D.; Arendt, M. F.; Yau, S. L.; Bell, C. M.; Mallouk, T. E., Growth and Characterization of Metal(Ii) Alkanebisphosphonate Multilayer Thin-Films on Gold Surfaces. *J Am Chem Soc* **1993**, *115* (25), 11855-11862.
10. Livingston, C.; Blanchard, G. J., Metal Ion-Dependent Interfacial Organization and Dynamics of Metal-Phosphonate Monolayers. *Langmuir* **2021**, *37* (15), 4658-4665.
11. Lee, H.; Kepley, L. J.; Hong, H. G.; Akhter, S.; Mallouk, T. E., Adsorption of Ordered Zirconium Phosphonate Multilayer Films on Silicon and Gold Surfaces. *J Phys Chem-US* **1988**, *92* (9), 2597-2601.
12. Kim, H. N.; Keller, S. W.; Mallouk, T. E.; Schmitt, J.; Decher, G., Characterization of zirconium phosphate polycation thin films grown by sequential adsorption reactions. *Chemistry of Materials* **1997**, *9* (6), 1414-1421.

13. Cao, G.; Lynch, V. M.; Swinnea, J. S.; Mallouk, T. E., Synthesis and Structural Characterization of Layered Calcium and Lanthanide Phosphonate Salts. *Inorg Chem* **1990**, *29* (11), 2112-2117.
14. Cao, G.; Lee, H.; Lynch, V. M.; Mallouk, T. E., Synthesis and structural characterization of a homologous series of divalent-metal phosphonates,  $MII(O_3PR)_2 \cdot nH_2O$  and  $MII(HO_3PR)_2$ . *Inorg Chem* **1988**, *27* (16), 2781-2785.
15. Cao, G.; Hong, H. G.; Mallouk, T. E., Layered Metal Phosphates and Phosphonates - from Crystals to Monolayers. *Accounts of Chemical Research* **1992**, *25* (9), 420-427.
16. Byrd, H.; Snover, J. L.; Thompson, M. E., Mechanistic Studies of Film Growth of Zirconium Bis(Phosphonate) Monolayer and Multilayer Thin-Films - These Things Grow Darned Flat. *Langmuir* **1995**, *11* (11), 4449-4453.
17. Kohli, P.; Rini, M. C.; Major, J. S.; Blanchard, G. J., Elucidating the balance between metal ion complexation and polymer conformation in maleimide vinyl ether polymer multilayer structures. *J Mater Chem* **2001**, *11* (12), 2996-3001.
18. Kohli, P.; Blanchard, G. J., Applying polymer chemistry to interfaces: Layer-by-layer and spontaneous growth of covalently bound multilayers. *Langmuir* **2000**, *16* (10), 4655-4661.
19. Kohli, P.; Blanchard, G. J., Design and demonstration of hybrid multilayer structures: Layer-by-layer mixed covalent and ionic interlayer linking chemistry. *Langmuir* **2000**, *16* (22), 8518-8524.
20. Horne, J. C.; Blanchard, G. J., Structural mediation of interlayer excitation transport in zirconium-phosphonate multilayers. *J Am Chem Soc* **1999**, *121* (18), 4427-4432.
21. Bakiamoh, S. B.; Blanchard, G. J., Surface second harmonic generation study of layer order in self-assembled multilayers. *Abstr Pap Am Chem S* **2001**, *221*, U90-U91.
22. Bakiamoh, S. B.; Blanchard, G. J., Demonstration of oriented multilayers through asymmetric metal coordination chemistry. *Langmuir* **1999**, *15* (19), 6379-6385.
23. Baumler, S. M.; Reidy, T. M.; Blanchard, G. J., Diffusional motion as a gauge of fluidity and interfacial adhesion. Supported alkylphosphonate monolayers. *J Colloid Interf Sci* **2016**, *468*, 145-155.
24. Soumpasis, D. M., Theoretical-Analysis of Fluorescence Photobleaching Recovery Experiments. *Biophys J* **1983**, *41* (1), 95-97.

25. Segur, J. B.; Oberstar, H. E., Viscosity of Glycerol and Its Aqueous Solutions. *Ind Eng Chem* **1951**, *43* (9), 2117-2120.

## **Chapter 5: Conclusions and Future Work**

The overall goal of this work was to determine if MP films exhibit surface fluidity and if modifications to the monolayers increase the fluidity of the se films, with the focus being on the following research questions.

1. Do ZP films exhibit surface fluidity?

The work highlighted in Chapter Two shows that ZP films do exhibit surface fluidity where FRAP measurements with both a tethered and an untethered chromophore showed translational movement of the monolayer constituents.

2. How does metal ion charge and identity effect the surface fluidity of MP films?

Six different MP monolayers were synthesized with several metal ions. Zr(IV), In(III), Mg(II), Ca(II), Ni(II), and Co(II) were used. No significant difference in translational diffusion of a tethered chromophore was observed for MP layers with varying metal ions (Table 5-1). This signifies that while the metal ion complexation dynamics does play a role in the fluidity of the film, changing the identity and charge of the metal ion didn't affect the diffusion of the tethered chromophore.

**Table 5-1.  $D_T$  values for MP monolayers with a tethered chromophore.**

Surface	Diffusion constant ( $D_T$ ) $\mu\text{m}^2/\text{s}$
Mg(II)- $\text{O}_3\text{P}-\text{C}_8\text{H}_{16}-\text{PO}_3\text{H}$	$0.20 \pm 0.10$
Co(II)- $\text{O}_3\text{P}-\text{C}_8\text{H}_{16}-\text{PO}_3\text{H}$	$0.32 \pm 0.26$
Ni(II)- $\text{O}_3\text{P}-\text{C}_8\text{H}_{16}-\text{PO}_3\text{H}$	$0.34 \pm 0.27$
Ca(II)- $\text{O}_3\text{P}-\text{C}_8\text{H}_{16}-\text{PO}_3\text{H}$	$0.49 \pm 0.40$
In(III)- $\text{O}_3\text{P}-\text{C}_8\text{H}_{16}-\text{PO}_3\text{H}$	$0.52 \pm 0.11$
Zr(IV)- $\text{O}_3\text{P}-\text{C}_8\text{H}_{16}-\text{PO}_3\text{H}$	$0.49 \pm 0.22$

While the tethered chromophore system exhibited no significant difference between MP films made with different metals, the untethered system showed a dependence on metal ion oxidation state (Table 5-2). MP monolayers formed with divalent metal ions exhibited lower  $D_T$  values than monolayers formed using In(III), which had a higher  $D_T$  value than Zr(IV). The main differences between these films are the oxidation state of the metal and, possibly, the packing density.

**Table 5-2. Average  $D_T$  values for MP monolayers with an untethered chromophore.**

Surface	$D_T$ ( $\mu\text{m}^2/\text{s}$ )
Mg(II)- O <sub>3</sub> P-C <sub>8</sub> H <sub>16</sub> -PO <sub>3</sub> H	3.33 ± 0.97
Co(II)- O <sub>3</sub> P-C <sub>8</sub> H <sub>16</sub> -PO <sub>3</sub> H	2.85 ± 0.78
Ni(II)- O <sub>3</sub> P-C <sub>8</sub> H <sub>16</sub> -PO <sub>3</sub> H	2.00 ± 0.45
Ca(II)- O <sub>3</sub> P-C <sub>8</sub> H <sub>16</sub> -PO <sub>3</sub> H	1.30 ± 0.56
In(III)- O <sub>3</sub> P-C <sub>8</sub> H <sub>16</sub> -PO <sub>3</sub> H	0.63 ± 0.17
Zr(IV)- O <sub>3</sub> P-C <sub>8</sub> H <sub>16</sub> -PO <sub>3</sub> H	0.31 ± 0.10

3. How does end group identity effect the surface fluidity of MP films?

Variation of the  $\omega$ -terminal functionality of the monolayers were seen to have limited influence on constituent diffusional properties. A slight increase in the aliphatic chain length did not change the translational diffusion behavior of the untethered chromophore contained in the monolayers. Removing the  $\omega$ -terminal phosphonate group decreases the mobility of the untethered chromophore in the monolayer, suggesting that MP monolayer organization is

dominated by the phosphonate density at the surface of the support. Metal ion capping of MP monolayers provided some evidence for slightly enhanced monolayer organization.

This work has the potential to move in many different directions. The Blanchard group does significant work with Langmuir-Blodgett (LB) films, including fluidity measurements. Previously, the fluidity of metal-phosphonate monolayers that mimicked a phospholipid has been described (Figure 5-1).<sup>16</sup> Directly comparing the fluidity of LB films and MP films is an obvious direction for this work to take by either creating MP monolayers using the phospholipid or synthesizing LB monolayers using bisphosphonates.

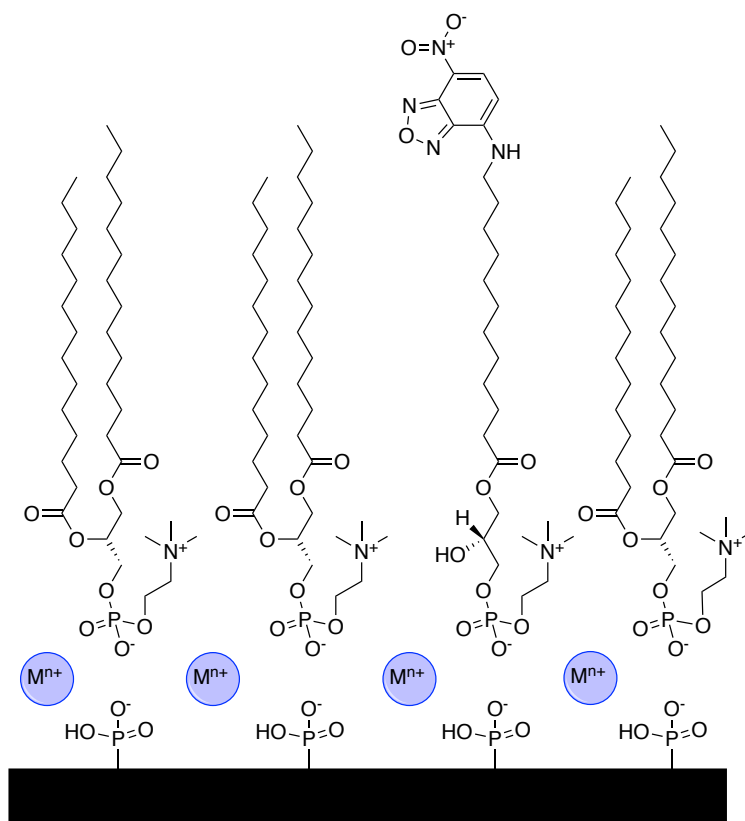


**Figure 5-1. Structure of LB film incorporating a metal, phospholipid (1,2-dimyristoyl-sn-glycero-3-phosphcholine), and a tethered chromophore.**

MP films are known for their stability with many multilayers.<sup>24</sup> Exploring the effect of increased layers on diffusional behavior within the multilayer structure could be a new direction for this project. Mixed metal systems with different metal represented in subsequent layers have been reported in the literature<sup>4</sup> and after determining the effect of multilayers fluid-like properties, making mixed metal systems offers an expansive next step.

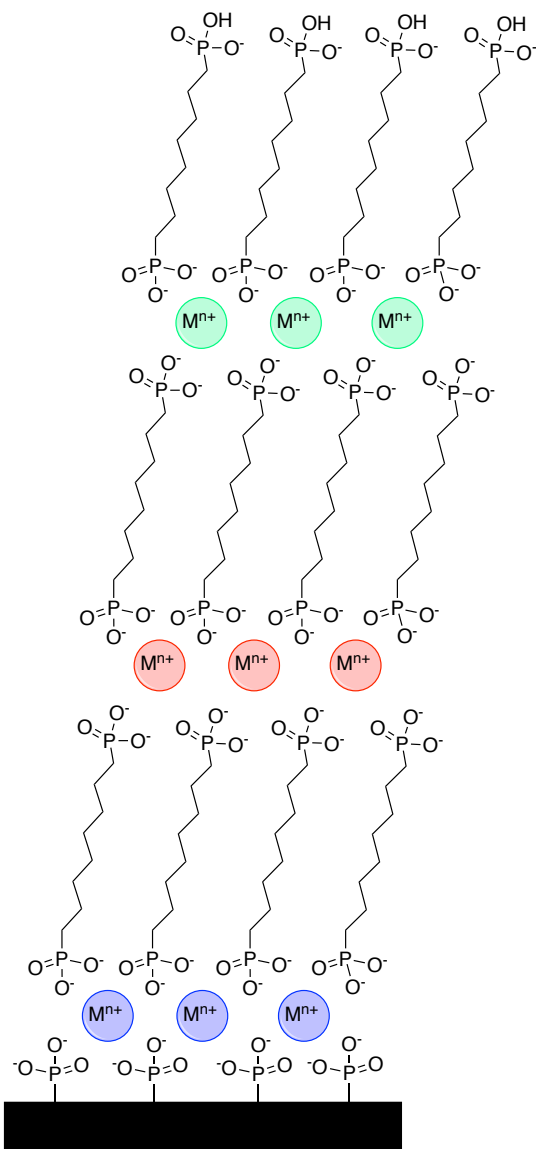


**Figure 5-2. Scheme of mixed metal MP multilayer.**

Currently in the Blanchard group, the electrochemical properties of thin films are being investigated. The electrochemical properties of MP films could also be of interest. If MP films are electrochemically stable, this opens up new applications, with the possibility of creating a film with tunable fluidity depending on the charge on the metal ion.

## **REFERENCES**

## REFERENCES

1. Baumler, S. M.; Reidy, T. M.; Blanchard, G. J., Diffusional motion as a gauge of fluidity and interfacial adhesion. Supported alkylphosphonate monolayers. *J Colloid Interf Sci* **2016**, *468*, 145-155.
2. Lee, H.; Kepley, L. J.; Hong, H. G.; Akhter, S.; Mallouk, T. E., Adsorption of Ordered Zirconium Phosphonate Multilayer Films on Silicon and Gold Surfaces. *J Phys Chem-Us* **1988**, *92* (9), 2597-2601.
3. Akhter, S.; Lee, H.; Hong, H. G.; Mallouk, T. E.; White, J. M., Structural characterization of multilayer metal phosphonate film on silicon using angular-dependent x-ray photoelectron spectroscopy. *Journal of Vacuum Science & Technology A* **1989**, *7* (3), 1608-1613.